NTNU
Norwegian University of
Science and Technology

Short circuit capacity improvement techniques for low voltage distribution grid.

Adrien Sélim Karoui

Master of Science in Electric Power Engineering
Submission date: June 2018
Supervisor: Kjetil Uhlen, IEL

Norwegian University of Science and Technology
Department of Electric Power Engineering

Abstract

Some part of the Norwegian low voltage distribution grid suffers from voltage dips during short term events such as motor start and short circuit fault. Since these voltage dips can lead to violation of the admissible voltage range for some second, it is needed to identify mitigation solutions to maintain the voltage within acceptable limits. The scope of this master thesis consists in the modelling of a small part of the low voltage distribution grid and to model and compare 2 technologies that are able to regulate the voltage at some nodes of the grid. The first technology developed by the company Magtech^{AS}, is the Magnetic Voltage Booster (MVB) based on the Magnetic Controllable Inductor technology. A model is developed, and its performances are compared to the well-known, power electronic based STATCOM solution. Three phases transient simulation of the modelled grid are run with motor start and short circuit contingencies. Based on the results of the simulations, the two performances are compared to characterize the MVB performances.

Acknowledgments

This work brings an end to my 5 years of engineering studies and therefore I would like to thank with this few words, the persons who have contributed directly or indirectly to my engineer training.

First of all, I would like to thank the University of Liège and the Norwegian University of Science and Technology for giving me the opportunity to perform this master thesis. In particular, I express my gratitude to Professor Kjetil Uhlen from NTNU who supervised me during the 5 months in Trondheim.

I also thank Santiago Sanchez from NTNU who's door was always opened for enriching advice and support. In addition, I would like to thank warmly David Fellner for his sharp eye on my work.

Finally, I would like to thank my family and my friends for theirs support during this 5 study years.

June 2018, Trondheim

Adrien Karoui

List of Abreviation

OLTC	On Load Tap Changer Transformer
MVB	Magnetic Voltage Booster
MCI	Magtech Controllable Inductor
DAE	Differential Algebraic Equations
STATCOM	Static Compensator
FACTS	Flexible Alternating Current Transmission System
VSC	Voltage Source Converter
SPWM	Space Vector Pulse Width Modulation
PLL	Phase Locked Loop
PI	Proportional- Integrator

List of Figures

List of Tables

Contents

Chapter 1

Introduction

Some part of the Norwegian distribution grid in rural area appeared to suffer from annoying voltage dips according to consumers complaints. These voltage dips may sometimes lead the voltage the admissible voltage range. This is usually the case when for example small industrial company such as sawmill start theirs motors several times throughout the day. Another problem which has been reported by the distribution network operator is the low short circuit capacity at the end of long radials feeders in rural areas. In case of short circuit fault, some protection devices may not operate properly because of the low short circuit current sensed by theses protection devices. When these problems occur, the voltage can remain below the admissible limit for seconds hindering the proper functioning of the supplied load. Especially, grid supplied electronic device may be altered.

In order to tackle this voltage issue, several voltage mitigation regulation solutions exist to improve voltage control: The On Load Tap Changer transformer (OLTC), shunt capacitor, power electronics. The two first solution are to slow to control and restore the voltage as their activation takes place after several seconds (6 to 30 seconds), when the faults are sudden and motor transients last 2 to 4 seconds. The latter are therefore considered as short-term events. Furthermore, the voltage will stabilize back once the motor speed has reached nominal speed. The reactive power compensation by power electronic is fast and reliable but its cost remains expensive preventing its widespread deployment. In today's grid, it is therefore marginally adopted solution.

In the year 2001, a new technology of reactive compensation has been developed and proposed by the company Magtech^{AS}. It is based on the magnetic controllable inductor technology. The latter belongs to the series compensation device category and in comparison to a STATCOM is characterized by a much lower amount of power electronic and mechanical equipment which can be considered as an advantage for an intensive use. Additionally, this technology is capable of a fast-dynamic response and is already implemented in some area of Norway and Sweden distribution grids. Therefore, the scope of this thesis consists in comparing, through transient simulations, the behaviour of the variable inductor technology with a shunt compensation device, namely a static compensator, based on the voltage profile during short circuit and motors start transients.

This thesis is structured in 7 chapters. Chapter 2 is dedicated to the modelling of the two electrical networks used in the simulations as test bed. The software environment is also briefly presented. Chapter 3 focuses on the working principle of an induction motor and its modelling for transient simulation. Chapter 4 and 5 describe respectively the working principle and the modelling process of the controllable inductor and the STATCOM technology. Chapter 6 presents and analyze the simulations results of the two devices during motor start and to short circuit events. Finally, a conclusion on the simulation results of the two voltage regulation solutions is drawn in Chapter 7.

Chapter 2

System topology and Simulation Environment

In this chapter, the two electric networks *Case Network* and *Test Network* used in this work are presented as well as the software environment adopted for the simulations. In the sequel, the model of the different elements that compose the two grids are described and the value of the numerical parameters given according to the data received from the grid company TrønderEnergi. Finally, the result of the power flow for the *Case Network* is presented and validated with the *MATLAB* Toolbox *MATPOWER*[1].

2.1 Case Network

The case network represented in Figure 2.1, is composed of one Thevenin equivalent network with a rated voltage level of 22kV RMS[1]. This voltage source is connected to the main busbar $BB1t$ at a rated voltage level of 230 V RMS through a power transformer TF_B1_B1t supplying the consumption side connected to busbar $B1t$. The consumption side has a radial structure and for the sake of clarity, is divided into 3 zones: A, B and C and respectively powered by the feeders[2] '$BB1t - BA1$', '$BB1t - BB1$' and '$BB1t - BC1$'. The loads connected to the end of each feeder are denoted with 'LXi where Xi denoted the busbar reference at which a load is connected.

[1]The voltage is always assumed line to ground RMS in the sequel of this thesis, otherwise specified.
[2]Feeder '$X - Y$' corresponds to the link between Bus X with Bus Y

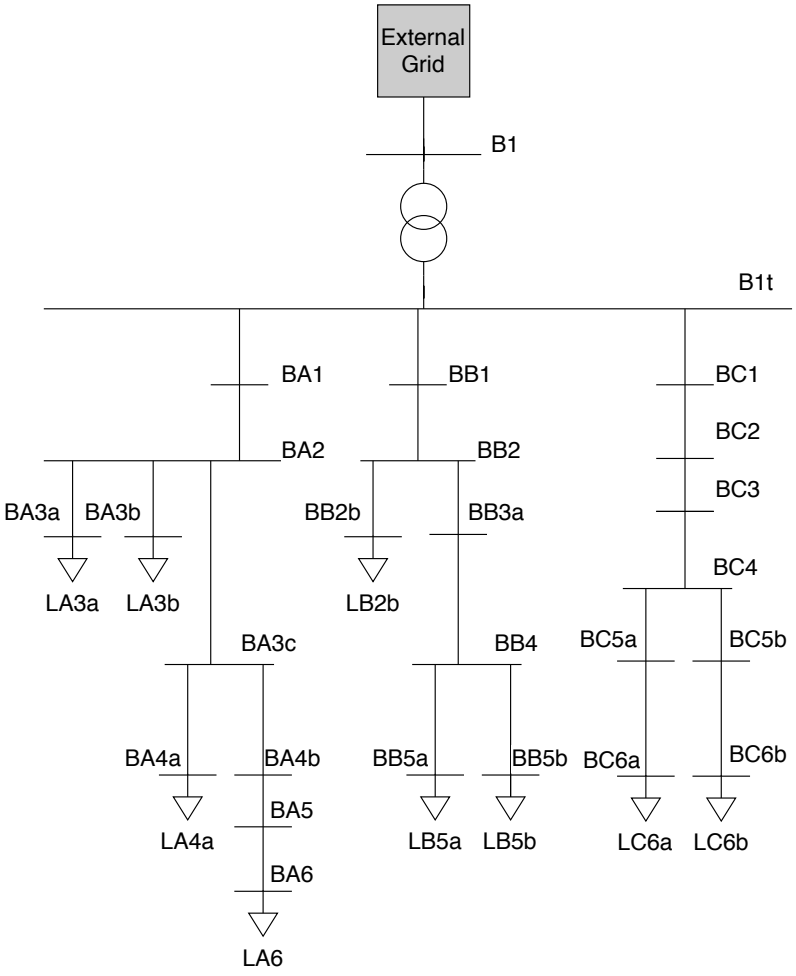

Figure 2.1: Schematic of the case network which is a anonymized portion of the TrønderEnergi grid.

2.2 Test Network

In order to test and simulate the behaviour of the different voltage compensating methods, a 4 buses system has also been set up and the corresponding topology can be found in Figure 2.2. This simpler system is composed of an external grid connected to the bus B_{HV} with rated voltage of 22 kV, a power transformer 22/0.23 kV linking bus B_{HV} with bus B_{LV}. A feeder has also been inserted between bus B_{LV} and bus B_{Load} to easily control the short power strength at B_{Load}.

The bus B_{Load} feeds three loads: two static loads respectively denoted by *Load* and *Load*2 and one squirrel cage induction machine denoted by $Motor$.

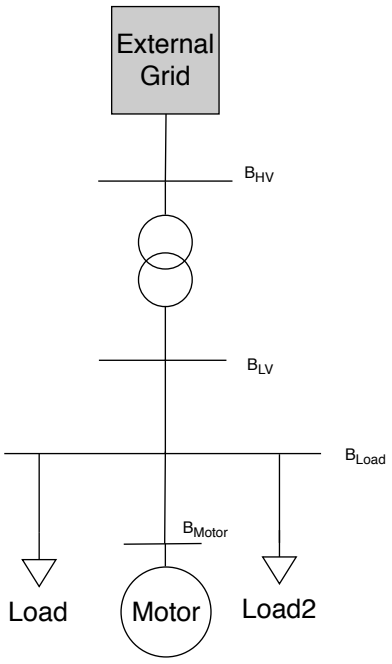

Figure 2.2: Schematic of the test network. This radial network is composed of one external grid, a power transformer and 3 loads. *Load* and *Load*2 are directly connected to bus B_{Load} while the motor is connected to B_{Load} through a feeder.

2.3 Simulation Software and Computational Environment

The transient simulations of the network are performed using the combined utilization of *Simscape*® and *Simulink*® within the *MATLAB*® software environment. The two first mentioned software are respectively used in this work to simulate the different transient phenomena and to model the different control laws that have been implemented in each controller of the compared compensating devices.

As previously mentioned, *Simscape*® is a scientific computational tool that allows the modelling of different physical domains. In this work, there are electrical and mechanical. Next to construction of the model by the user, the compilation of the *Simscape*® file operates according to the process[2] shown in Figure 2.3.

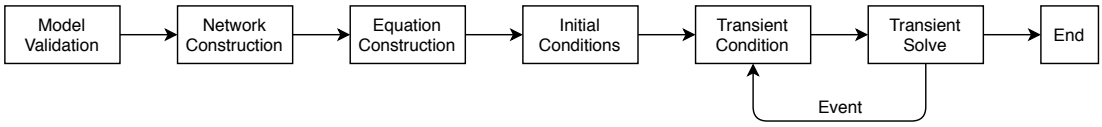

Figure 2.3: Simscape compilation process

The solver used to simulate the behaviour of the electrical grid is *ode23t*. This solver belongs to the trapezoidal integration methods[3] and is considered as the solver of choice when it comes to solve a system of Differential Algebraic Equations (DAE)[4].

2.4 Network Components

Ideal Voltage Source

The power generation of the network is modelled using an ideal voltage source able to produce perfectly balanced 3 phases AC voltage. Consequently, during the power flow computation and the transient simulation, the busbar plays the role of 'slack bus' meaning that its voltage magnitude and voltage angle are specified and assumed constant during the complete simulation time. Equations (2.1a-c) represent this ideal 3 phases voltage sources.

$$v_{a,sl} = \sqrt{2}V_n \; cos(\omega \; t + \theta_{sl}) \tag{2.1a}$$

$$v_{b,sl} = \sqrt{2}V_n \; cos(\omega \; t + \theta_{sl} + \frac{2\pi}{3}) \tag{2.1b}$$

$$v_{c,sl} = \sqrt{2}V_n \; cos(\omega \; t + \theta_{sl} + \frac{4\pi}{3}) \tag{2.1c}$$

where $v_{i,sl}$ $(i \in \{a, b, c\})$, θ_{sl} and V_n represent respectively the 3 phases instaneaous voltages, the voltage angles and the line-to-ground RMS voltages.

Medium Voltage Equivalent Network

To get rid of the high voltage side during the transient simulation of the Case network, the external grid and the power transformer have been replaced by a Thevenin equivalent. This consists of a Thevenin voltage source V_{th} and a Thevenin impedance Z_{th} that represent the sensitivity to reactive power infeed of the voltage at different nodes of the grid. This concept is illustrated with the QV characteristic in Figure 2.4.

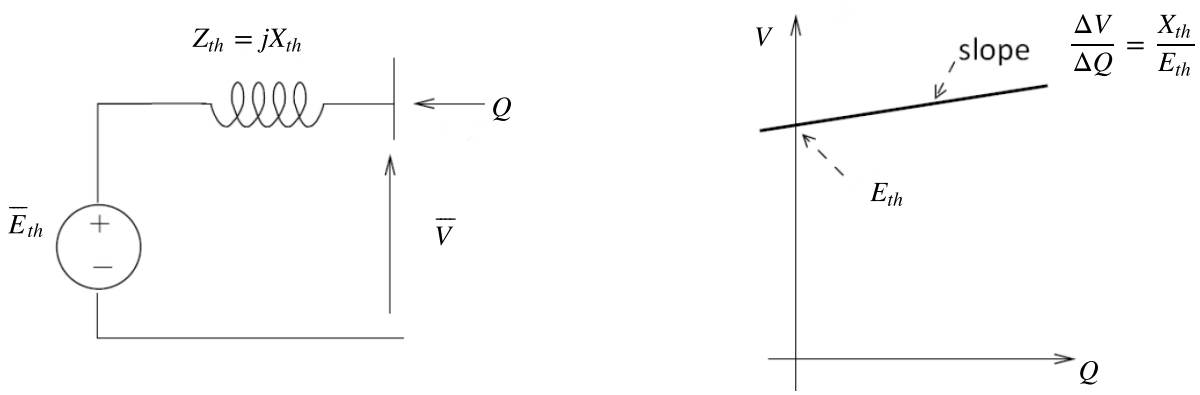

Figure 2.4: QV characteristic[5]

Based on the slope of the QV characteristic, one can see that when reactive power is injected into the equivalent network, the voltage increases and the rate at which the voltage increases is dependant, as a first approximation, on the ratio $\frac{X_{th}}{E_t h}$ and therefore on the short circuit power. However, this assertion is under the hypothesis that Thevenin impedance is purely reactive which is fairly the case in medium voltage distribution grid[5].

The assumed stiffness of the grid relative to the voltage is characterized by two parameters: The Short circuit ratio S_{sc} and the $\frac{R_{th}}{X_{th}}$ ratio. These variables are represented in Equation (2.2a-c).

$$Z_{th} = R_{th} + jX_{th} \tag{2.2a}$$

$$\phi = \frac{X_{th}}{R_{th}} \tag{2.2b}$$

$$R_{th} = \frac{U_n^2}{S_{sc}\sqrt{1+\phi^2}} \tag{2.2c}$$

where U_n, R_{th} and X_{th} are respectively the line to line voltage, the per phase Thevenin resistance and reactance.

Transmission Line

The transmission line model used in the simulation software is given in Figure 2.5[6]. The self-resistance and mutual inductance R_m and L_m are neglected and the value of the parameters used in the modelled grid for the resistance R, the inductance L and the line-to-ground and line-to-line capacitance C_g and C_l are given in Appendix A. This 3-phase model is described in $\alpha\beta\gamma$ formalism[7] using the Clarke transformation detailed in Appendix C.

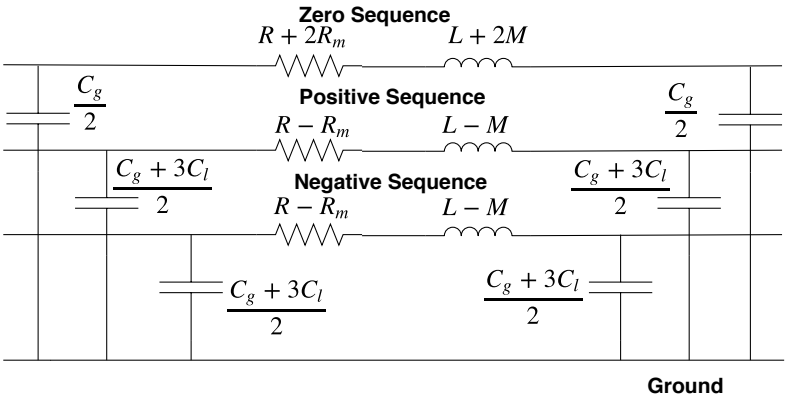

Figure 2.5: Transmission line model in the positive-negative-zero sequence formalism

The simulations are performed in the 'abc' formalism and thus the Clarke transform $\mathbf{C}$ and its inverse $\mathbf{C}^{-1}$ are applied respectively at the sending and the receiving end of the transmission line model. This is illustrated in Figure 2.6 and in Equation (2.3a-b) where $\mathbf{V}_{send}^{\alpha\beta\gamma}$ and $\mathbf{V}_{send}^{abc}$ denoted respectively the vector of 3 phase phasors in the 'abc' and '$\alpha\beta\gamma$' formalism. Finally, the transfer matrix $\mathcal{T}_{\alpha\beta\gamma}$ makes the link between the sending and the receiving end quantities in the '$\alpha\beta\gamma$' sequence as shown in Equation (2.4).

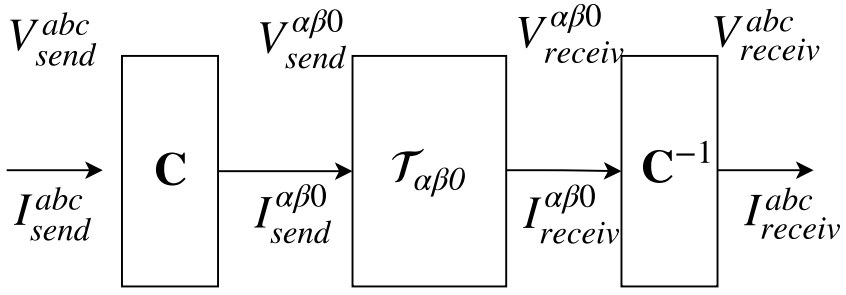

Figure 2.6: Sending-Receiving end model of the trnasmission line model expressed in the $\alpha\beta\gamma$ formalism

$$\mathbf{I}_{send}^{\alpha\beta\gamma} = \mathbf{C}\ \mathbf{I}_{send}^{abc} \qquad \mathbf{V}_{send}^{\alpha\beta\gamma} = \mathbf{C}\ \mathbf{V}_{send}^{abc} \tag{2.3a}$$

$$\mathbf{I}_{receiv}^{\alpha\beta\gamma} = \mathbf{C}\ \mathbf{I}_{receiv}^{abc} \qquad \mathbf{V}_{receiv}^{\alpha\beta\gamma} = \mathbf{C}\ \mathbf{V}_{receiv}^{abc} \tag{2.3b}$$

$$\begin{bmatrix} \mathbf{V}_{send}^{\alpha\beta\gamma} \\ \mathbf{I}_{send}^{\alpha\beta\gamma} \end{bmatrix} = \mathcal{T}_{\alpha\beta\gamma} \begin{bmatrix} \mathbf{V}_{receiv}^{\alpha\beta\gamma} \\ \mathbf{I}_{receiv}^{\alpha\beta\gamma} \end{bmatrix} \tag{2.4}$$

Power Transformer

The power transformer used in the*Simscape*® model is mounted in a Yyn0 configuration with 100 kVA rating power. This transformer is modelled with its 3 phase equivalent circuit but for the sake of clarity, a per phase equivalent model is shown in Figure 2.7. The parameters specified in the *Simscape*® model are:

- the primary and secondary nominal phase voltages V_1 and V_2
- the primary and secondary leakage inductances L_{l1}, L_{l2}
- the primary and secondary leakage resistances L_{l1}, L_{l2}
- the magnetizing reactance X_m
- the nominal frequency f_{nom} at which the transformer operates.

The per unit value of the cited parameter expressed in the 100 kVA base can be found in Table 2.1. Since the base primary and secondary voltages $V_{1,base}$ and $V_{2,base}$ are respectively equal to the nominal voltages, the per unit transformer ratio $\overline{n}$ is equal to 1.

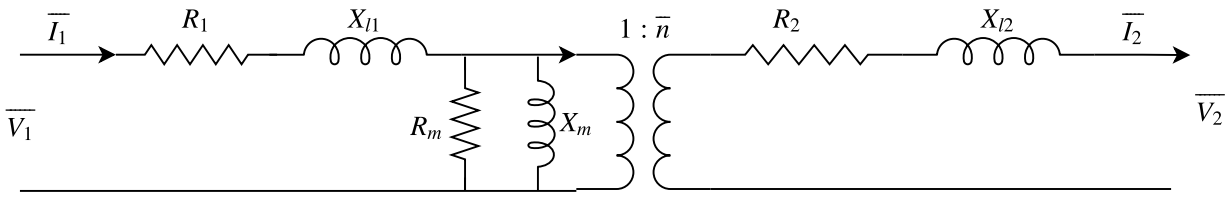

Figure 2.7: Per phase equivalent model of the power transformer.

Parameter	X_{l1},X_{l2}	R_1,R_2	X_m	R_m	$\overline{n}$
Value [pu]	0.001	0.01	500	500	1

Table 2.1: Characteristic parameters of the power transformer given in pu.

Load

The power consumption modelled in the two networks is made up of two types of load as shown in Figure 2.8: a static voltage-dependent load and a squirrel cage induction motor. These two load type represent a faithful image of the real type of loads.

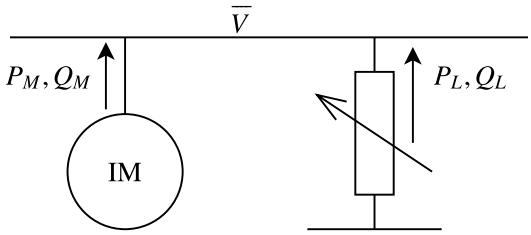

Figure 2.8: Typical aggregated load model.

The static load is modelled by an algebraic relation between the active and reactive power injection and the voltage and the load terminal. It is assumed that the load is invariant with respect to the frequency. From the two previous mentioned parameters, the voltage dependency is described in Equation (2.5a-b) according to the exponential model[8] of a load. The value of a and b have been assumed equal to 2 which corresponds to a constant impedance load.

$$P_L = P_{L0}\left(\frac{V}{V_0}\right)^a = P_{L0}\left(\frac{V}{V_0}\right)^2 \tag{2.5a}$$

$$Q_L = Q_{L0}\left(\frac{V}{V_0}\right)^b = Q_{L0}\left(\frac{V}{V_0}\right)^2 \tag{2.5b}$$

The 3 phases squirrel cage induction machine model is defined by:

- a rated power P_{rated},
- a number n of pairs of poles,
- a rated voltage V_{rated},
- a rated electrical frequency f_{rated},
- electrical pulsation ω_s and rotor speed ω_r
- a rotor inertia constant J and motor slip $s = \frac{\omega_s - \omega_r}{\omega_s}$,
- and electrical equivalent resistance and reactance R_{eq} X_{eq}.

In steady state operation, the induction machine can be modelled with an equivalent circuit[9] shown in Figure 2.9 where X_m and X_{eq} correspond respectively to the magnetizing reactance and to the leakage stator and rotor reactance.

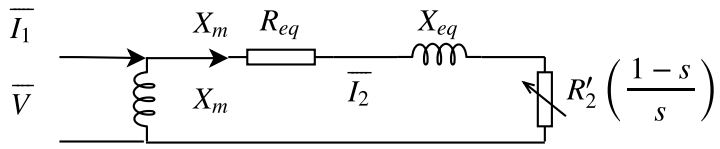

Figure 2.9: Equivalent electrical circuit of the induction machine.

The joules losses originating from the stator and from the rotor are condensed into R_{eq} while the mechanical load is represented inside $R'_2\frac{1-s}{s}$.

Short-Circuit & Circuit Breaker

The short circuit modelled in the network takes the form of a 3 phases fault with a grounded neutral as it can be seen in Figure 2.10. These faults are the most severe. In the *Simscape*® simulation environment, the fault is characterized by two parameters as input: the faulted phase-neutral and faulted ground neutral resistance $R_{\phi n}$ and R_{ng}.

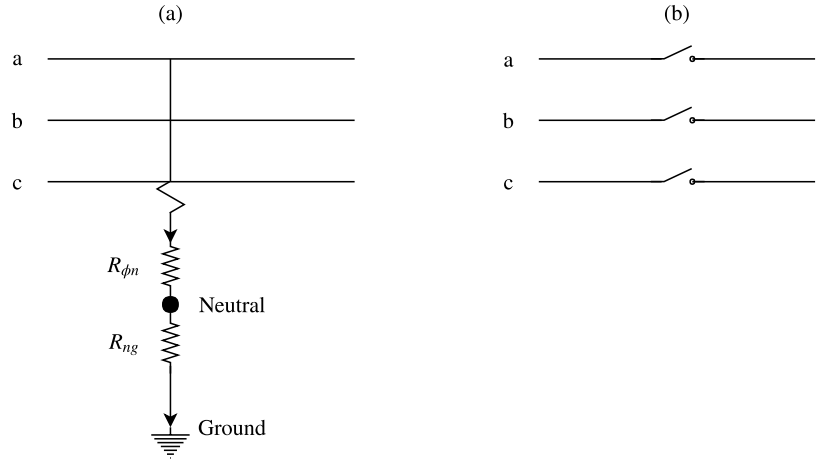

Figure 2.10: Model of the three phase fault (a) and the ideal phase circuit breaker (b)

In order to clear the fault, a circuit breaker model of *Simscape*® has been chosen and is modelled as a 3 phase ideal switch as shown in Figure 2.10. It should be mentioned that the built-in model of the circuit breaker monitors the 3 phase instantaneous current and opens the switch whenever the phase current cross zero as it is the case in a real circuit breaker.

Measurement Device

In order to gather the measurement data ($V_{RMS}, I_{RMS}, P_{3\phi}, Q_{3\phi}$) at different locations in the network, an ideal measurement device has been implemented with the *Simscape*® block *pq_measurement.ssc*. This block senses continuously the instantaneous voltage and current and performs a running time integration as shown in Equation (2.6a-b) to obtain the RMS value of the phase voltage and phase current.

$$V_{RMS} = \sqrt{\frac{1}{T}\int_{t}^{t+T} v_a(\tau)^2 d\tau} \tag{2.6a}$$

$$I_{RMS} = \sqrt{\frac{1}{T}\int_{t}^{t+T} i_a(\tau)^2 d\tau} \tag{2.6b}$$

where T represents the integration time, assumed equal to 20 ms. According to the instantaneous power theory, the value of the 3 phases active and reactive power $P_{3\phi}$ and $Q_{3\phi}$ are obtained using the relation[10] of Equation (2.7).

$$P_{3\phi} = v_a i_a + v_b i_b + v_c i_c \tag{2.7a}$$

$$Q_{3\phi} = \frac{1}{\sqrt{3}}\left[(v_b - v_c)i_a + (v_c - v_a)i_b + (v_a - v_b)i_c\right] \tag{2.7b}$$

2.5 Power flow validation

The model validation of the network used in the *Simscape*® environment is assessed by performing a power flow computation with the help of an independent toolbox $MATPOWER$ and by comparing the obtained result with the ones received from the distribution network company TrøndEnergy. These results are presented in Table 2.2.

	Bus Voltage [pu]		
Bus Name	**TrønderEnergi**	**MATPOWER**	**Simscape**
B1T	0,99	0.9927	1
BA6	0,94	0.9753	0.984
BA4a	0,96	0.9815	0.989
BA3b	0.96	0.9820	0.989
BA3a	0.96	0.9817	0.989
BB5a	0.95	0.9799	0.988
BB3b	0.96	0.9828	0.99
BC6a	0.98	0.9886	0.99
BC6b	0.98	0.9833	0.99

Table 2.2: Power flow result comparison between the result received by the company, the toolbox MATPOWER and the Simscape environment.

From the result obtained in Table 2.2, one can observe that both the MATPOWER and the Simscape software does not perfectly match the voltage obtained from the grid company TrønderEnergi. However, the Matpower results are slightly more accurate than Simscape results. This is most likely due to the topology simplification made in the *Simscape*® software where the external grid as well as the transformer have been replaced by a Thevenin equivalent. Nevertheless, the tendency of the voltage at the different result nodes of the network is the same for the three softwares.

Chapter 3

Motor Modeling and Starting

In order to analyze the voltage transient during motor start, an induction machine model has to be chosen. This model is derived from a typical induction machine used in the sawmill industry. First the physics of the induction machine is briefly described then the implemented model of the motor is derived. Finally, the evolution of the active and reactive power as well the electromagnetic torque are presented.

3.1 Physics of the induction machine

The induction machine is an electromechanical device that is composed of a stator and a rotor. The mechanical load connected to the rotor is driven by the magnetic interaction between the stator and the rotor magnetic fluxes. The stator flux is generated by the 3 phases current flowing through the stator winding while the rotor flux is generated by induced current of the rotor flowing through the rotor windings.

The rotor motion results from the balance between the electromagnetic torque T_e created by the magnetic rotating flux in the airgap and the mechanical torque T_m applied on the shaft by the load. A mechanical analogy of this interaction in illustrated in Figure 3.1.

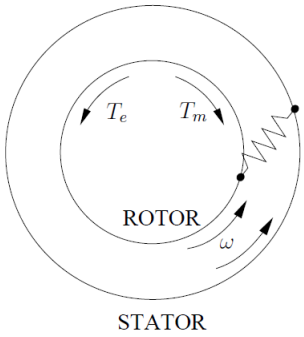

Figure 3.1: Mechanical analogy of the torque interaction relative to the rotor motion where $\omega = s\omega_s$ represent the mechanical angular speed of the rotor.

3.2 Mathematical Model

The system of equations used to model the dynamic behaviour of the induction machine is given in Equation (3.1)-(3.3)[8]. Originally, these equations are represented in the static reference frame of the stator and the rotor respectively. In order to deal with non-oscillating quantities, these equations are passed from a static reference frame to a rotating reference frame, called *dq synchronous reference frame* using the Park Transformation. This new reference frame rotates at the angular speed ω_s.

$$v_{ds} = R_s\ i_{ds} - \omega_s\ \psi_{qs} + \frac{d\psi_{ds}}{dt} \tag{3.1a}$$

$$v_{qs} = R_s\ i_{qs} + \omega_s\ \psi_{ds} + \frac{d\psi_{qs}}{dt} \tag{3.1b}$$

$$v_{dr} = R_r\ i_{dr} - s\omega_s\ \psi_{qr} + \frac{d\psi_{dr}}{dt} \tag{3.1c}$$

$$v_{qr} = R_r\ i_{qr} + s\omega_s\ \psi_{dr} + \frac{d\psi_{qr}}{dt} \tag{3.1d}$$

where v_{ds} and v_{qs} correspond respectively to the stator d and q voltage components while v_{dr} and v_{qr} represent the d and q rotor voltage component.
The self and mutual flux linkage in the rotor and in the stator are related to the current through the following Equation (3.2) :

$$\psi_{ds} = L_{ss}\ i_{ds} + L_m\ i_{dr} \tag{3.2a}$$

$$\psi_{dr} = L_m\ i_{ds} + L_{rr}\ i_{dr} \tag{3.2b}$$

$$\psi_{qs} = L_{ss}\ i_{qs} + L_m\ i_{qr} \tag{3.2c}$$

$$\psi_{qr} = L_m\ i_{qs} + L_{rr}\ i_{qr} \tag{3.2d}$$

The rotor motion is modelled using the swing Equation (3.3) where T_e and T_m correspond respectively to the electromagnetic and mechanical torque.

$$J\frac{d\omega_r}{dt} = T_e - T_m \tag{3.3}$$

The mechanical torque is considered to be a quadratic function of the rotor speed[11]. The ABC model with A=1, B=C=0 is chosen.

$$T_m = T_{m0}\left(A\ \omega_r^2 + B\ \omega_r + C\right) = T_{m0}\omega_r^2 \tag{3.4}$$

where T_{mo} is the value of the torque when the rotor is at nominal mechanical speed $\omega_r = 1[pu]$. The parameters of the motor used for the transient simulation are shown in Table 3.1.

Parameter	**Symbol**	**Value**	**Unit**
Nominal apparent power Ratings	S_m	12000	VA
Rated Voltage RMS (line-to-ground)	V_n	230	V
Number of pair of pole	n_{poles}	1	1
Stator resistance	R_s	0. 258	pu
Stator leakage inductance	L_{ls}	0.0930	pu
Referred rotor resistance	$R_{r'}$	0.0145	pu
Referred rotor leakage inductance	$L_{lr'}$	0.0424	pu
Magnetizing inductance	L_m	1.7562	pu
Inertia	J	0.07	kg m^2

Table 3.1: Parameters value used for the squirrel cage induction machine.

3.3 Torque speed Characteristic

The torque speed characteristic of the squirrel cage induction machine is depicted in Figure 3.2. This curve is obtained by representing the electromagnetic Torque T_e against the rotor speed ω_r when the circuit breaker of the induction machine is close to grid. This method of starting the motor is called 'Direct On line Start'. As it can be seen in Figure 3.2, when the grid voltage is applied at 0.8 second, there is a high reactive power consumption from the induction machine. This is due to the short circuit behaviour of the machine at rest and due to the induced magnetization of the rotor winding to create the electromagnetic torque T_e. After the mechanical speed ω has reached its nominal value, the reactive power consumption is reduced drastically. However, some reactive power is still drawn in order to keep the airgap magnetized and keep the synchronization between the electromagnetic and the mechanical torque.

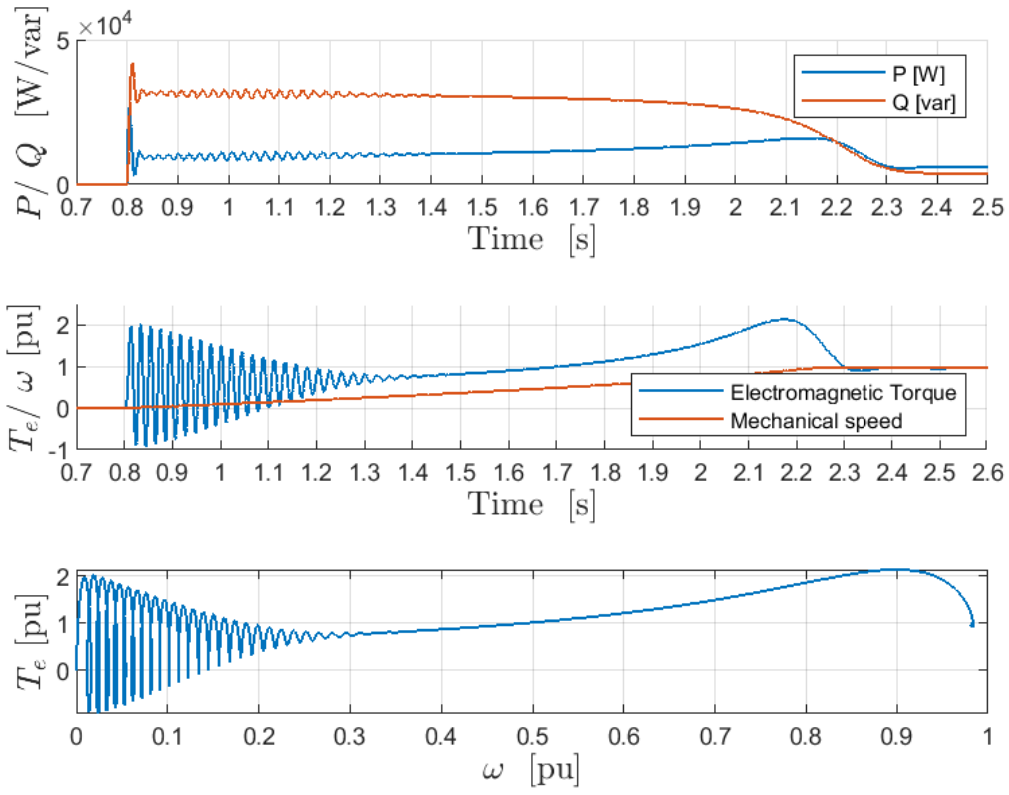

Figure 3.2: Evolution of the electromagnetic torque when the motor is started from zero initial rotor speed and when the stator voltage is not regulated to 1 pu.

Chapter 4

The Magnetic Voltage Booster

This chapter is dedicated to the modelling and to the analysis of the first compensating device, namely, the magnetic voltage booster (MVB). First, the working principle of this technology is introduced and the implementation to achieve the voltage control at the secondary side is explained. Next, the steady state characteristic of the device is derived from its dynamic behaviour and in the last section, a control law is proposed and validated.

4.1 MagtechAS™ Technology

The company MagTechAS™[12] has developed and patented a voltage regulation device for the low voltage distribution grid. The per phase electric design of the MVB is shown in Figure 4.1. From the electrical connection, one can first observe that the system is highly similar to a power transformer. In fact, the device consists of an auto transformer and a normal transformer. The primary side voltage of the auto transformer is considered as the input voltage and the secondary side as the output or controlled voltage. The lower node of the auto transformer is galvanically coupled with a magnetic variable inductor (MCI) through a power transformer (neglected in the sequel). The value of the variable inductance is controlled with a direct current (dc) that has been beforehand rectified from the secondary side of the auto transformer.

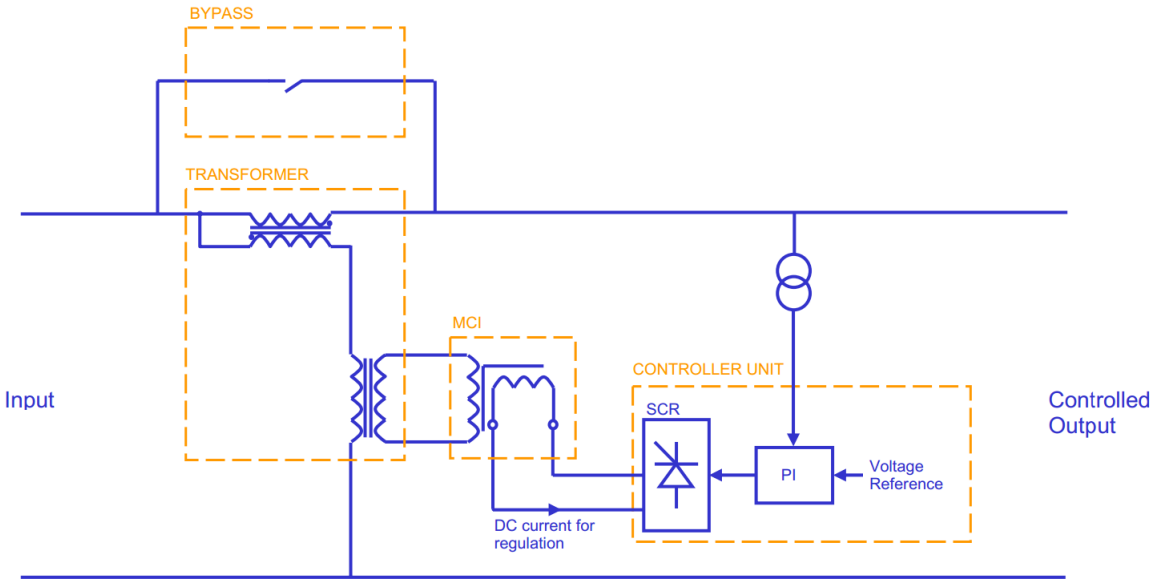

Figure 4.1: Block diagram of the MVB device and his associated controller.

4.2 Working principle

The core of the MVB technology is the Magnetic Controllable Inductor (MCI). The voltage across the MCI is controlled by changing the inductance value of the inductor [13].

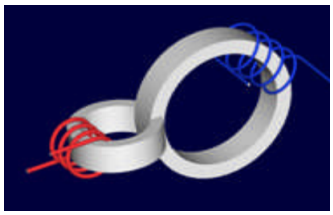

Figure 4.2: Three-dimensional view of the magnetic controllable inductor [14].

The MCI is made up of 2 orthogonal coupled magnetic cores around which 2 coils, a main and auxiliary, are wounded. The main magnetic flux flowing through the main core is produced by the alternating current i flowing into the blue winding (blue coloured in Figure 4.2). This main flux will interact with a controllable flux that is produced by a dc current i_{dc} flowing into the auxiliary winding (red coloured in Figure 4.2). The consequence of this flux interaction is the creation of a variable virtual air gap. This virtual air gap is created by the local modification of the magnetic flux distribution in the core depending on the dc current intensity flowing in the auxiliary winding[13].

The inductance of the main coil is related to the reluctance of the core according to Equation (4.3). This expression is derived as follow:

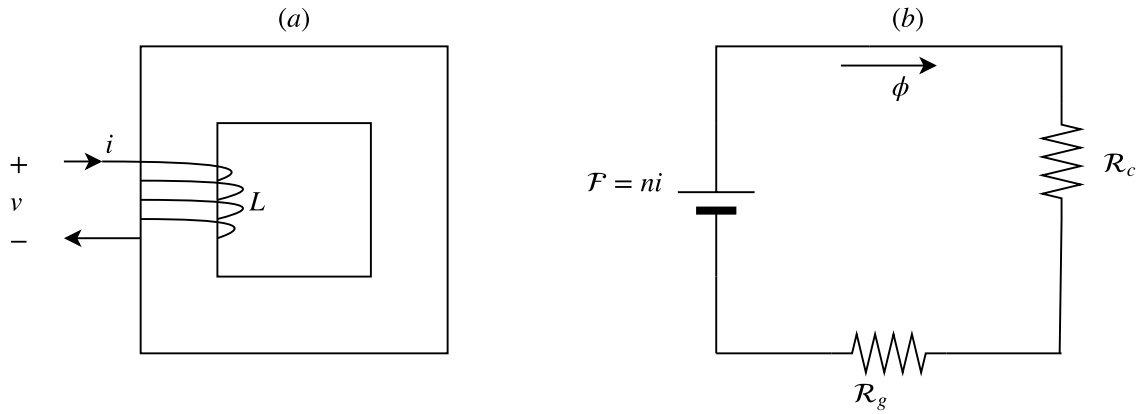

Figure 4.3: Inductor wounded around a magnetic core (a) and the corresponding magnetic equivalent circuit (b).

Starting from the magnetic circuit of a inductor wounded around a magnetic core as represented in Figure 4.3, the magnetomotive force $\mathcal{F}$ is given by Equation (4.1).

$$\mathcal{F} = ni = (\mathcal{R}_c + \mathcal{R}_g)\,\phi \tag{4.1}$$

where n is the number of winding of the inductor, i is the dc current flowing through the inductor, $\mathcal{R}_c$ and $\mathcal{R}_g$ are respectively the reluctance of the core and the virtual airgap and ϕ is the magnetic flux density flowing through the magnetic core.

Furthermore, the voltage law of an inductor is given by Equation (4.2).

$$v = -\frac{d\psi}{dt} = -n\frac{d\phi}{dt} = -\frac{n^2}{(\mathcal{R}_c + \mathcal{R}_g)}\frac{di}{dt} = -L\frac{di}{dt}\ , \tag{4.2}$$

where ψ is the total flux embraced by the inductor. The leakage flux that composes the total flux ψ is neglected. Then, replacing Equation (4.1) in Equation (4.2), one obtains the expression for the inductance L:

$$L = \frac{n^2}{(\mathcal{R}_c + \mathcal{R}_g)}, \tag{4.3}$$

where n is the number of turns of the main winding, $\mathcal{R}_c$ corresponds to the reluctance of the core region where the auxiliary winding little affects the main core flux and $\mathcal{R}_g$ corresponds to region of the core where the virtual air gap is created. Therefore, the inductance of the MCI can be controlled using the dc current i_{dc} injected into the auxiliary coil.

4.3 Per-phase modelling

The per phase model diagram of the MVB device is given in Figure 4.4. In this model, some assumptions have been made with respect to the original electric design of Figure 4.1 and these are listed hereafter:

1. Auto transformer is assumed ideal.
2. Galvanic decoupling of MCI with the auto transformer is neglected.
3. MCI inductance has infinitely fast dynamic.
4. Power electronic dynamics of the rectifier is neglected.
5. Each phase voltage is controlled individually.

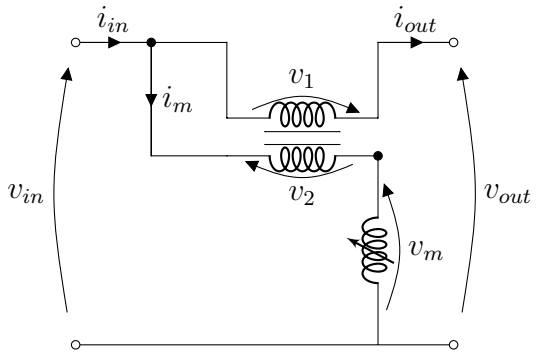

Figure 4.4: Per phase electrical model of the MVB device

In Figure 4.4, the variables v_{in} and i_{in} represent the input voltage and currents while v_{out} and i_{out} are the output voltage and currents. The voltage v_1 and v_2 represent respectively the primary and the secondary voltage across the auto-transformer while v_m and i_m correspond respectively to the voltage and current across and through the variable inductor L_m. It is also assumed that the auto transformer is ideal in term of losses and that the magnetic coupling between v_1 and v_2 is neglected.

Dynamic model

Using the electric model derived in Figure 4.4, the dynamic model of the MVB is established and implemented in the *Simscape*® modelling environment and presented in Appendix D. This system is of algebraic differential equation type. Equations (4.4 a-g) are obtained with the voltage and current balance at the only node of the electric circuit.

$$i_{in} = i_m + i_{out} \tag{4.4a}$$
$$i_m = \frac{1}{n} i_{out} \tag{4.4b}$$
$$v_m = L_m \frac{di_m}{dt} \tag{4.4c}$$
$$v_2 = n v_1 \tag{4.4d}$$
$$v_{out} = v_{in} + v_1 \tag{4.4e}$$
$$v_{in} = v_m + v_2 \tag{4.4f}$$
$$v_{out} = z i_{out} \tag{4.4g}$$

where n and z are respectively the ideal auto-transformer tap ratio and the load representing the right side of the MVB device.

Steady state model

In steady state operation, the dynamical system of equation can be passed into phasor notation assuming that the frequency is constant. By doing so, the steady state transfer function between v_{out} and v_{in} take the form:

$$MVB(s) = \frac{\overline{V}_{out}}{\overline{V}_{in}} = Z \frac{(1+n)}{nZ + \frac{jX_m}{n}} \tag{4.5}$$

This transfer function depends on the impedance Z, the value of the tap ratio n and as expected, on the variable reactance X_m. Thus, if n, Z and $\overline{V}_{in}$ are assumed constant, it is possible to increase (resp. decrease) $|\overline{V}_{out}|$ by decreasing (resp. increasing) X_m. This behaviour is illustrated in Figure 4.5 for different value of Z.
The base value used in the plot of the steady-state transfer function are shown in Table 4.1.

S_{base} [VA]	V_{base} [V]	I_{base} [A]	Z_{base} [Ω]
2000	230	2.89	79.35

Table 4.1: Base value used for computing the MVB transfer function. It should be noted that V_{base} corresponds to the phase to neutral RMS voltage and where $S_{base} = 3V_{base}I_{base}$

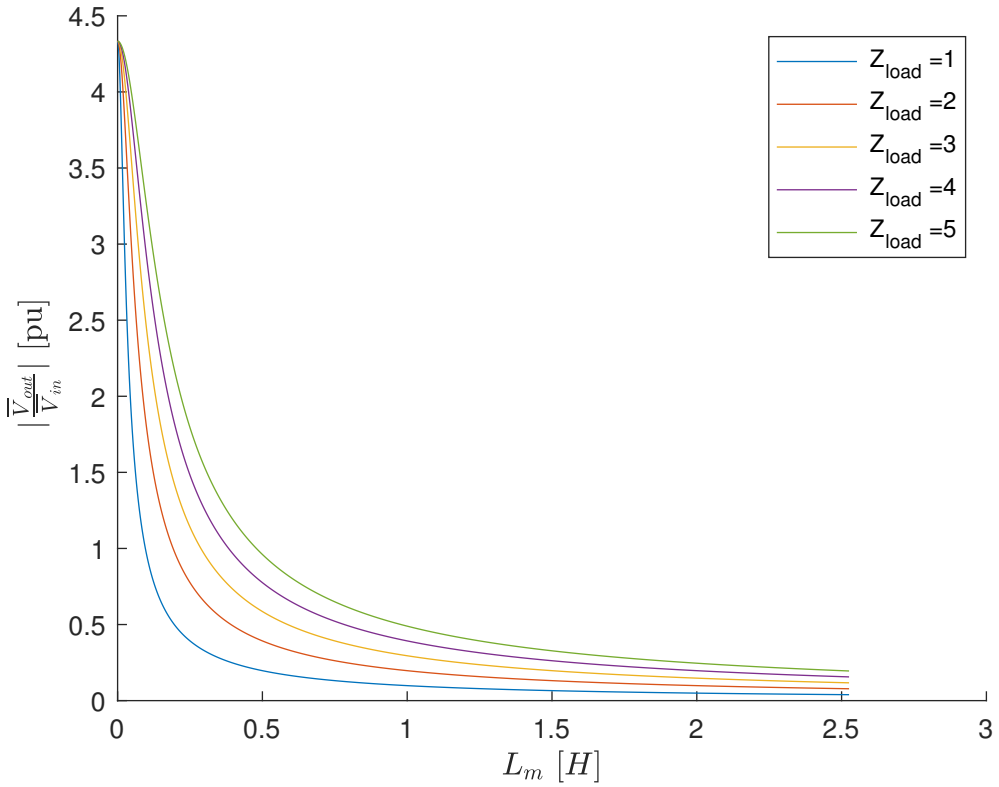

Figure 4.5: Magnitude of the SS transfer function when the variable inductance is changing for different value of load and when the auto transformer tap ratio is equal to 0.3 .

4.4 Control Law

The voltage v_{out} is controlled using a basic control system shown in Figure 4.6. The output voltage v_{out} is first measured and is processed to extract the RMS value V_{out}. Then, V_{out} is compared to the voltage set point V_{ref} and the error is cancelled using a proportional integral (PI) controller. The output of the PI controller becomes then the amount δL_m to add to the initial inductance L_m^{ini} to regulate the output voltage. It has to be mentioned that since the behaviour of the transfer function $MVB(s)$ is non-linear for high value of L_m, a saturation block has been added at the output of the second summation block Σ.

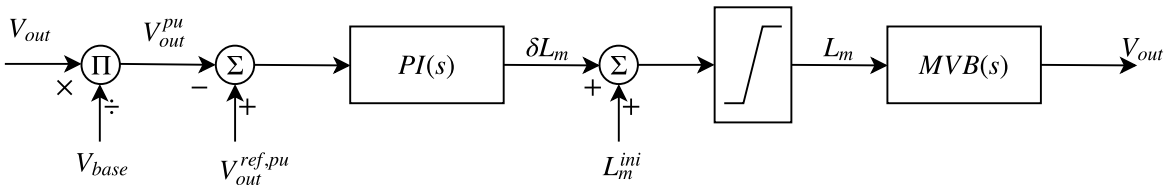

Figure 4.6: Diagram of the MVB controller.

The value of the PI controller gains k_p and k_i of Equation (4.6) for the two grids are given in Table 4.2. The tuning has been made such that the dynamic response of the MVB goes back to steady state after 150 ms according to the characteristic of the MVB device provided in Appendix B.

$$PI(s) = k_p + \frac{k_i}{s} \tag{4.6}$$

Grid	k_p	k_i
Test grid	-1	-100
Case grid	-0.05	-10

Table 4.2: PI gains value of the MVB controller

The validation of the control system has been made in the Test grid and the result is shown in Figure 4.7. The simulated scenario is a sequence of set point values for the voltage reference ($[1 - 1.05 - 1 - 0.95 - 1]$).The aim is to observe the correct dynamic of the MVB with respect to a set point modification.

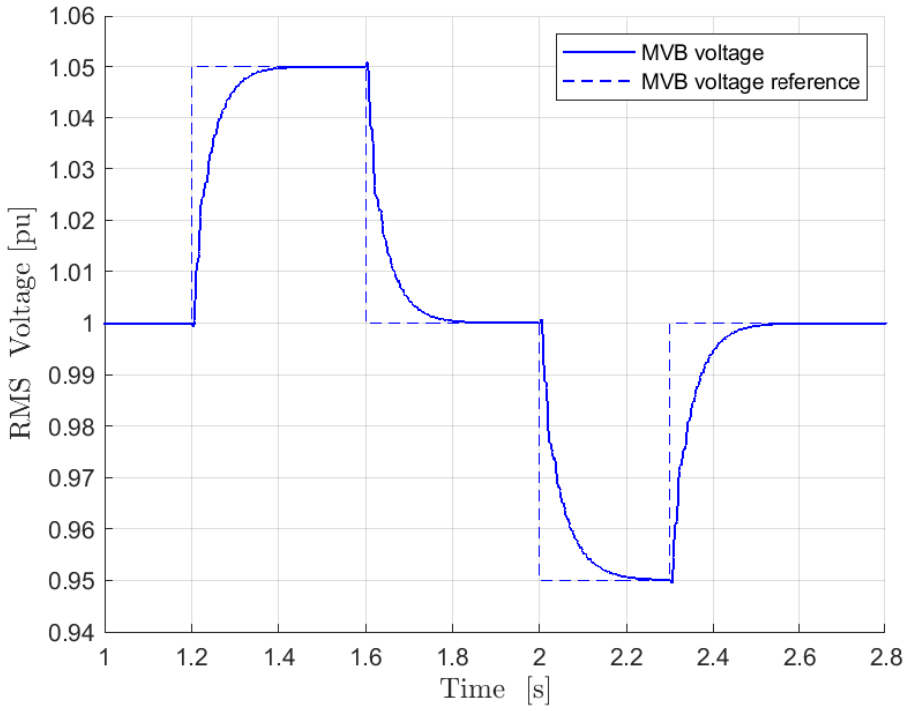

Figure 4.7: Test of the MVB control system by reference tracking simulation.

Chapter 5

Distribution Static Compensator

Chapter 5 analyses and models the distribution STATCOM which is in this work considered as the second solution to solve the voltage dips issues. First, the working principle a STATCOM is introduced and the major components are described. Then, some assumptions are presented in order to model and implement the device in the analysed grids. The mathematical formalism used to allow the voltage regulation at a location of the grid is described and the outer and inner control law are derived. Finally, the control behaviour of the modelled STATCOM is tested with some reference simulations.

5.1 Working Principle

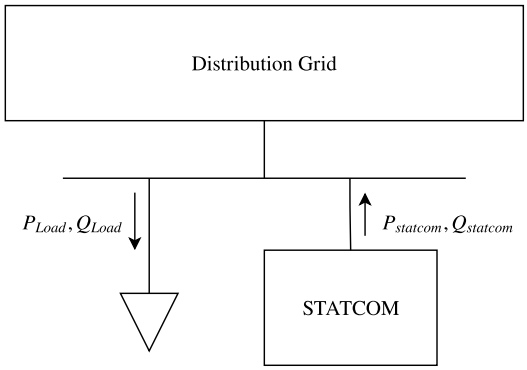

Figure 5.1: General STATCOM connection.

The working principle of the STATCOM as represented in Figure 5.1 relies on the combination of power electronic and filtering to generate a voltage waveform which is phase shifted with respect to the connected busbar. The power electronic generates a voltage waveform by converting a dc signal into an ac signal. The type of converter used in the analysed STATCOM is the Voltage Source Converter (VSC) since it can be assimilated as an ideal voltage source. The role of the controller is then to control the voltage magnitude and the phase

shift of the produced voltage waveform in order to inject the desired active and reactive power.

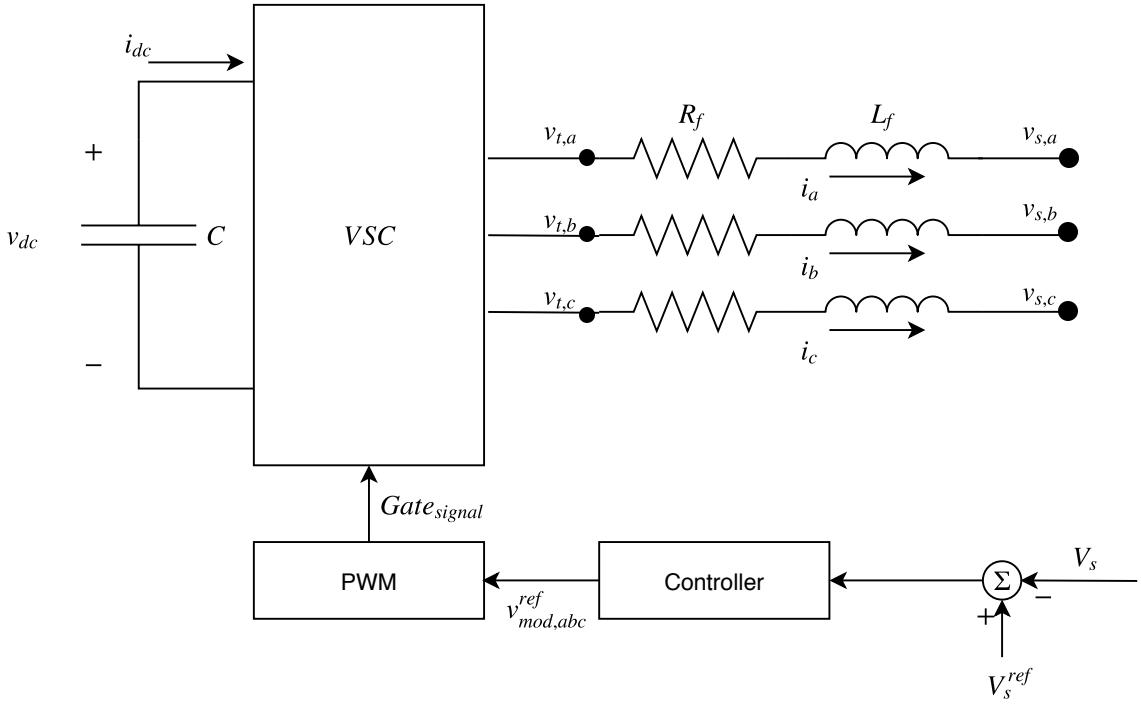

Figure 5.2: Structure of the STATCOM

The STATCOM structure, depicted in Figure 5.2, is organized in 4 parts: the first part is the DC capacitor C which has a constant DC voltage under the controller action. The second part is the VSC and the PWM modulator that are responsible for the generation of the voltage waveform. Then, a filtering inductance L_f is placed between the VSC busbar and the busbar of the grid in order to smooth the voltage waveform. Finally, the last part is the controller responsible of the voltage regulation and the PWM modulator.

5.2 Voltage Source Converter

The voltage source converter used in the STATCOM is depicted in Figure 5.3. This converter is a 3 phases 2 level converter composed of 6 thyristors switches. In this work, the switches are assumed ideal, meaning that each switch commutes instantaneously and the resistance that usually take into account the commutation losses is neglected. However, these switching losses can be included within the filtering resistance R_f.
The switching sequence responsible for generating the voltage waveforms $v_{t,a}$,$v_{t,b}$ and $v_{t,c}$ results from the Pulse Width Modulation technique. This technique consists in comparing a reference signal, also called the modulating signal v_m with amplitude V_M with a sawtooth carrier signal of constant amplitude V_c and frequency f_c as depicted in Figure 5.4.

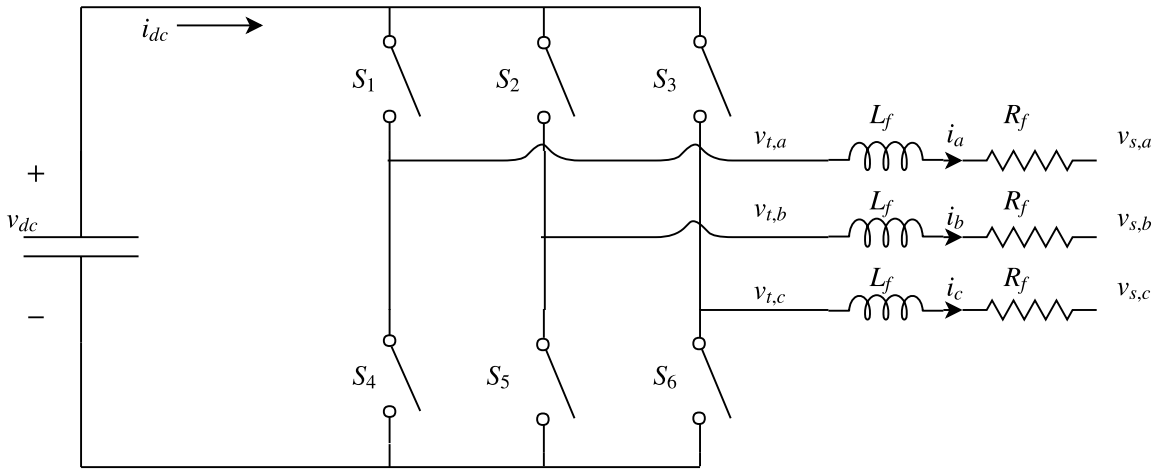

Figure 5.3: VSC 3 phase 2 level topology.

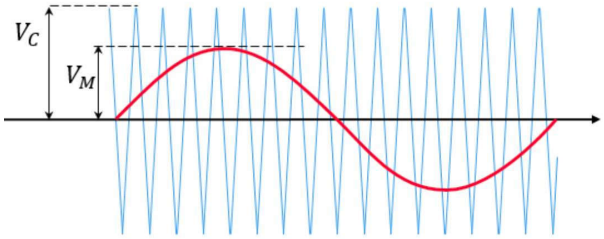

Figure 5.4: PWM modulation technique where V_M and V_C are respectively the amplitude of the modulating and sawthoot carrier signals[15].

From the signal depicted in Figure 5.4, the modulation index m is defined as $m = \frac{V_M}{V_C}$. This index is an image of the margin to the over modulation where the signal is not perfectly sinusoidal anymore but saturated on the extrema. It should be mentioned that with a conventional sinusoidal modulation signal, the over modulation occurs at m equal to 1. However, it is possible to increase this limits value up to $m = 1.15$ by using a different modulating signal $v_{mod,3}$ where the third harmonic of the fundamental sinusoidal signal is added[16]. The modified reference voltage is given in Equation (5.1) and the corresponding waveform is compared with the purely sinusoidal signal in Figure 5.5.

$$v_{mod,3} = \frac{2}{\sqrt{3}}\ m\ \left(sin(\omega\ t) + \frac{1}{6}\ sin(3\ \omega\ t)\right) \tag{5.1}$$

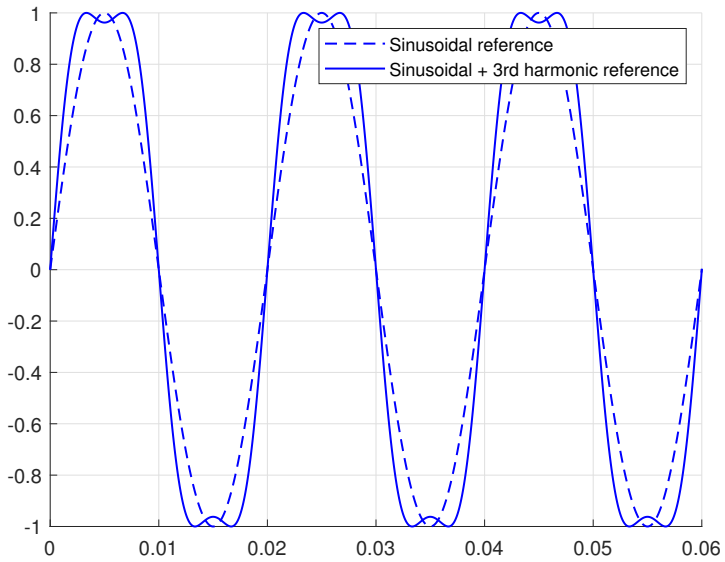

Figure 5.5: Comparison between sinusoidal and third harmonic injection reference signal for m=1.

5.3 Network equation

The modelling of the STATCOM has been implemented in the basis of the reference book[17]. In the sequel, the electrical circuit equations of Figure 5.3 are derived with the space phasor formalism described in Appendix C. Then, the Park transformation is applied in order to convert the different variables from the abc static reference frame into the rotating dq reference frame. This transformation has two advantages. The first one is that the complexity of the system is reduced since after transformation, only two equations are considered instead of 3. The second advantage is that all the previous oscillating variables are now constant in the dq rotating reference frame (assuming steady state). Here again, the dq rotating reference frame is explained in Appendix C.

Starting from the instantaneous value of the voltage and current:

$$v_{s,a} = \hat{V}_s cos(\omega_0 t + \theta_s) \tag{5.2a}$$

$$v_{s,b} = \hat{V}_s cos(\omega_0 t + \theta_s + \frac{2\pi}{3}) \tag{5.2b}$$

$$v_{s,c} = \hat{V}_s cos(\omega_0 t + \theta_s + \frac{4\pi}{3}) \tag{5.2c}$$

where $\hat{V}_s$, θ_s and ω_0 denoted respectively the voltage amplitude, the phase angle and the nominal pulsation. In order to obtain the system equation, the voltage law between the vsc node $v_{t,k}$ and the point of common coupling $v_{s,k}$ is derived in Equation (5.3)

$$\overrightarrow{v}_t - \overrightarrow{v}_d = L_f \frac{d\overrightarrow{i}}{dt} + R_f \overrightarrow{i} \tag{5.3}$$

where $\overrightarrow{v}_t$, $\overrightarrow{v}_s$ and $\overrightarrow{i}$ are the space phasor given by Equation (5.4)

$$\overrightarrow{v}_t(t) = \frac{2}{3}[v_{t,a}(t)e^{j0} + v_{t,b}(t)e^{j\frac{2\pi}{3}} + v_{t,c}(t)e^{j\frac{4\pi}{3}}] = \hat{V}_t e^{j\theta_t}e^{j\omega t} = \overline{V_t}e^{j\omega t} \tag{5.4a}$$

$$\overrightarrow{v}_s(t) = \frac{2}{3}[v_{s,a}(t)e^{j0} + v_{s,b}(t)e^{j\frac{2\pi}{3}} + v_{s,c}(t)e^{j\frac{4\pi}{3}}] = \hat{V}_s e^{j0}e^{j\omega t} = \overline{V_s}e^{j\omega t} \tag{5.4b}$$

$$\overrightarrow{i}(t) = \frac{2}{3}[i_a(t)e^{j0} + i_b(t)e^{j\frac{2\pi}{3}} + i_c(t)e^{j\frac{4\pi}{3}}] = \hat{I}e^{j\psi}e^{j\omega t} = \overline{I}e^{j\omega t} \tag{5.4c}$$

Equation (5.3) can be projected on the d and q axis by,

$$v_{dq,t}e^{j\rho} - v_{dq,s}e^{j\rho} = L_f\frac{d(i_{dq}e^{j\rho(t)})}{dt} + R_f i_{dq}e^{j\rho(t)}, \tag{5.5}$$

where the notation $x_{dq} = x_d + jx_q$ has been used and where $\rho(t)$ corresponds to the rotating angle locating the rotating dq reference frame with respect to the static axis of phase a. Developing the differential term of Equation (5.5), one gets:

$$v_{dq,t} - v_{dq,s} = L_f i_{dq}j\frac{d\rho(t)}{dt} + L_f\frac{di_{dq}}{dt} + R_f i_{dq}, \tag{5.6}$$

Moreover, a Phase-Locked Loop mechanism (PLL) is used to synchronize the angular speed $d\rho(t)/dt$ of the rotating dq reference frame with the angular speed ω_0 of the space phasor $\overrightarrow{v_s}$. Substituing $d\rho(t)/dt = \omega_0$ in Equation (5.6) and decomposing into real and imaginary part, Equation (5.7) are obtained.

$$L_f\frac{di_d}{dt} = \omega_0 L_f i_q - R_f i_d + v_{d,t} - v_{d,s} \tag{5.7a}$$

$$L_f\frac{di_q}{dt} = -\omega_0 L_f i_d - R_f i_q + v_{q,t} - v_{q,s} \tag{5.7b}$$

Furthermore, the VSC output voltages $v_{t,k}$ are related to the dc voltage v_{dc} through the modulating signal $m_k(t)$ (k=a,b and c) and these relations 5.8a-b can be also expressed in the dq rotating reference frame:

$$v_{t,d} = m_d\frac{v_{dc}}{2} \tag{5.8a}$$

$$v_{t,q} = m_q\frac{v_{dc}}{2} \tag{5.8b}$$

Equation (5.6) and (5.8) are then per unit using the base value represented in Table B.2 of Appendix B.

$$\frac{L_{f,pu}}{\omega_B}\frac{di_{d,pu}}{dt} = \omega_{pu}L_{f,pu}i_{q,pu} - R_{f,pu}i_{d,pu} - m_d v_{dc,pu} + v_{d,pu,s} \tag{5.9a}$$

$$\frac{L_{f,pu}}{\omega_B}\frac{di_{q,pu}}{dt} = \omega_{pu}L_{f,pu}i_{d,pu} - R_{f,pu}i_{q,pu} - m_q v_{dc,pu} + v_{q,pu,s} \tag{5.9b}$$

Since the aim of the controller is to regulate the current injection, it is required to decouple the system by defining 2 new variables u_d and u_q leading to the two independent ordinary differential equations. The Equation (5.10a-b). constitute then the basis for the controller implementation. The suffix $_{pu}$ will be omitted in the sequel of the modelling.

$$\frac{L_f}{\omega_B}\frac{di_d}{dt} = -R_f i_d + u_d \tag{5.10a}$$

$$\frac{L_f}{\omega_B}\frac{di_q}{dt} = -R_f i_q + u_q \tag{5.10b}$$

where u_d and u_q are given by Equation (5.11).

$$u_d = \omega L_f i_q + m_d v_{dc} - v_{d,s} \tag{5.11a}$$

$$u_q = -\omega L_f i_d + m_q v_{dc} - v_{q,s} \tag{5.11b}$$

5.4 PLL

The PLL mechanism in its general purpose is used to track the phase angle of an oscillating signal. In the case of the VSC controller, it is used to synchronize the d axis of the rotating dq reference frame with the space phasor of the voltage at the PCC node. To achieve the synchronization in the 3 phase system, a Park transform using controlled angle ρ is applied to the measured voltage space phasor $\overrightarrow{v_s}$. Then, the resulting q component of the measured signal is compared to zero and an error is computed. This error is cancelled using a PID controller that feeds a controlled oscillator to produce the synchronized angle ρ. This control system is illustrated in Figure 5.6 and used in the *Simscape*® model of Appendix C (STATCOM).

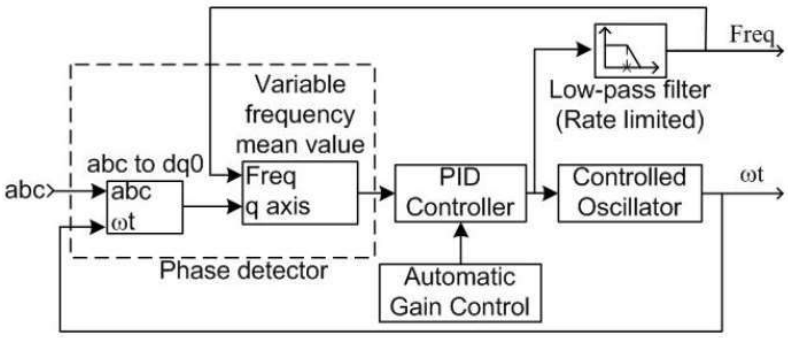

Figure 5.6: PLL controller used in the *Simscape*® model[18].

5.5 STATCOM Controller

The STATCOM Controller is composed of an inner and an outer controller. The inner control aims to control the STATCOM current injection by producing the voltage waveform v_t while the outer controller aims to control the dc bus voltage v_{dc} and the point of common coupling voltage V_{pcc}. The next sections present the respective block diagram of the different controller.

Inner Controller

The goal of the inner controller is to regulate the active and reactive current injection i_d and i_q. Therefore, two proportional integral controllers are used respectively to the control the input variable u_d and u_q. Figure 5.7 shows the block diagram implemented in the *Simulink*® model of the STATCOM.

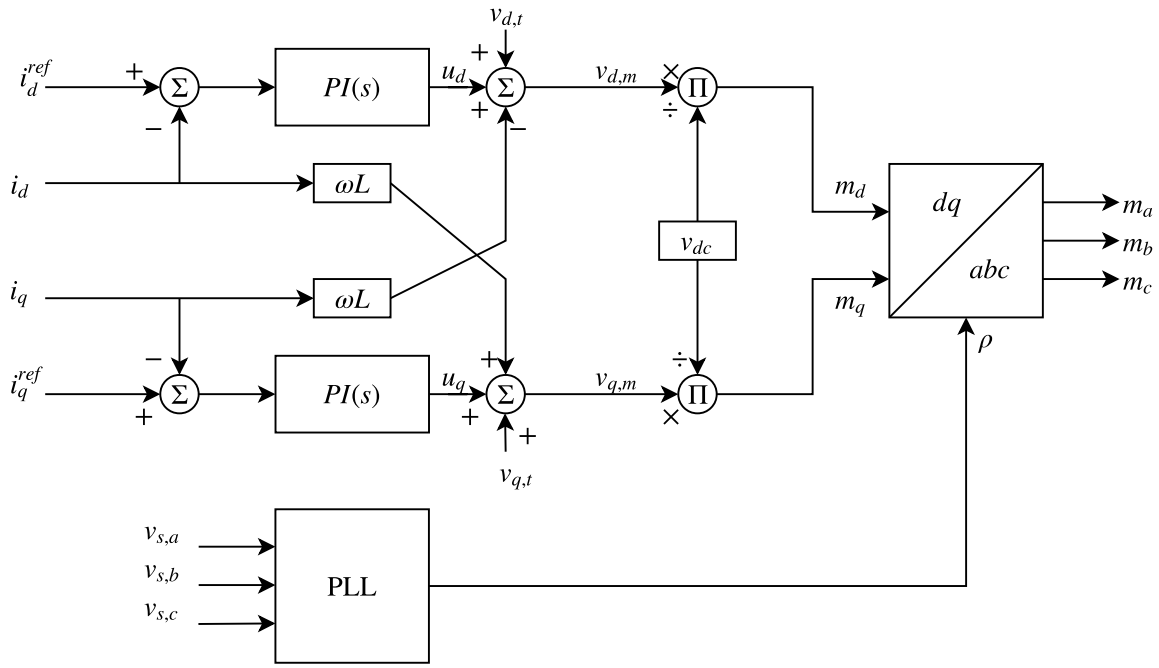

Figure 5.7: Block diagram of the STATCOM inner controller

Passing the Equation (5.11) and the PI controller in the Laplace domain, one obtains Equation (5.12) for the d axis where $L'_f = \frac{L_f}{\omega_B}$ is the redefined filtering inductance. It should be mentioned that the symmetry of the system of equation allows a same control tuning in the d as in the q axis. Therefore, the subscript $_d$ and $_q$ will be omitted for the gain tuning of the transfer function and gain parameters notations.

$$H_{VSC}(s) = \frac{1}{R_f} \frac{1}{1 + s\left(\frac{L'_f}{R_f}\right)} \tag{5.12a}$$

$$H^{in}_{PI}(s) = k^{in}_p + \frac{k^{in}_i}{s} \tag{5.12b}$$

The parameter k^{in}_p and k^{in}_i denoting the inner PI gains in the d an q axis are tuned using the Modulus Optimum technique described in Appendix B.

Outer Controller

Once the inner controller shows a proper and fast response with respect some reference changes, the active current i_d and i_q can be used to control the active and the reactive power injection of the statcom. Indeed, the expression of the active and reactive power in per unit during steady state operation in the dq rotating reference frame are given by Equation (5.13).

$$P_{statcom} = v_{d,s} i_d + v_{q,s} i_q = v_{d,s} i_d \tag{5.13a}$$

$$Q_{statcom} = -v_{d,s} i_q + v_{q,s} i_d = -v_{d,s} i_q \tag{5.13b}$$

Furthermore, the active power balance of the VSC system provide a relation between the dc voltage of the capacitor and the 3-phase active power while the reactive power injection is able to control the voltage magnitude at the point of common coupling.

$$v_{dc} i_{dc} = P_{statcom} = v_{d,s} i_d \tag{5.14}$$

Therefore, the active current controller (i_{d_ref}) is used to control the DC voltage of the capacitor and the reactive current i_{q_ref} is used to control the voltage magnitude at the STATCOM terminals. The block diagram for the regulation of the bus voltage and DC voltage is depicted in Figure 5.8 while the *Simulink*® models used for the STATCOM controller is shown in Appendix D.

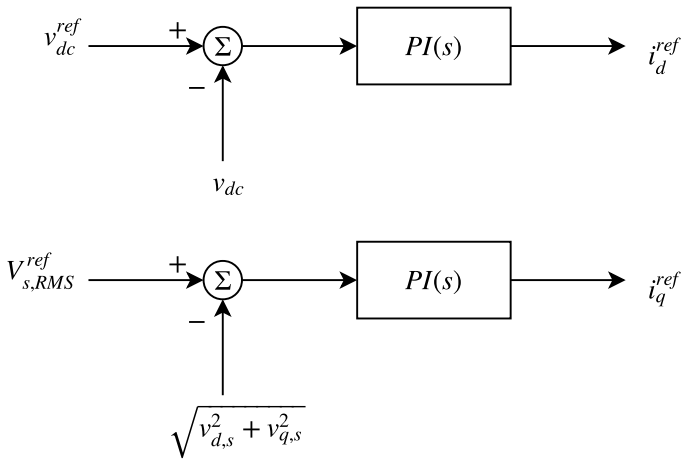

Figure 5.8: Block diagram of the STATCOM outer controller

5.6 Simulation

Design parameters

In order to test the proper functioning of the STATCOM, the parameter values of the filtering inductance L_f and resistance R_f as well as the capacitance of the DC capacitor C_{dc} and the switching frequency f_s have to be specified. The per unit and the normal unit are represented in Table 5.1.

Parameters	**Value [pu]**	**Value[Unit]**
L_f	0.5	0.0025 H
R_f	0.01	0.016 Ω
C_{dc}	10	0.0075 F
f_s	/	1000 Hz

Table 5.1: Design value of the parameters of the STATCOM

Inner controller reference tracking

The list of events used during the simulation in order to test the inner controller are represented in Table 5.2. The scenario represents an active power injection of 1 kW before a reactive power injection of 1 kvar.

Outer controller reference tracking

The outer controller is tested by changing the voltage reference. During the test, the list of voltage reference applied to the outer controller is shown in Table 5.3. It corresponds respectively to reactive production and reactive power absorption from the STATCOM.

Timing	Event [pu]
Initially	$i_d^{ref} = i_q^{ref} = 0$
t= 0.30 s	$i_d^{ref} = 0.2$
t= 0.70 s	$i_d^{ref} = 0$
t= 1.0 s	$i_q^{ref} = -0.2$
t= 1.30 s	$i_q^{ref} = 0$

Table 5.2: Event list of the inner controller test simulation.

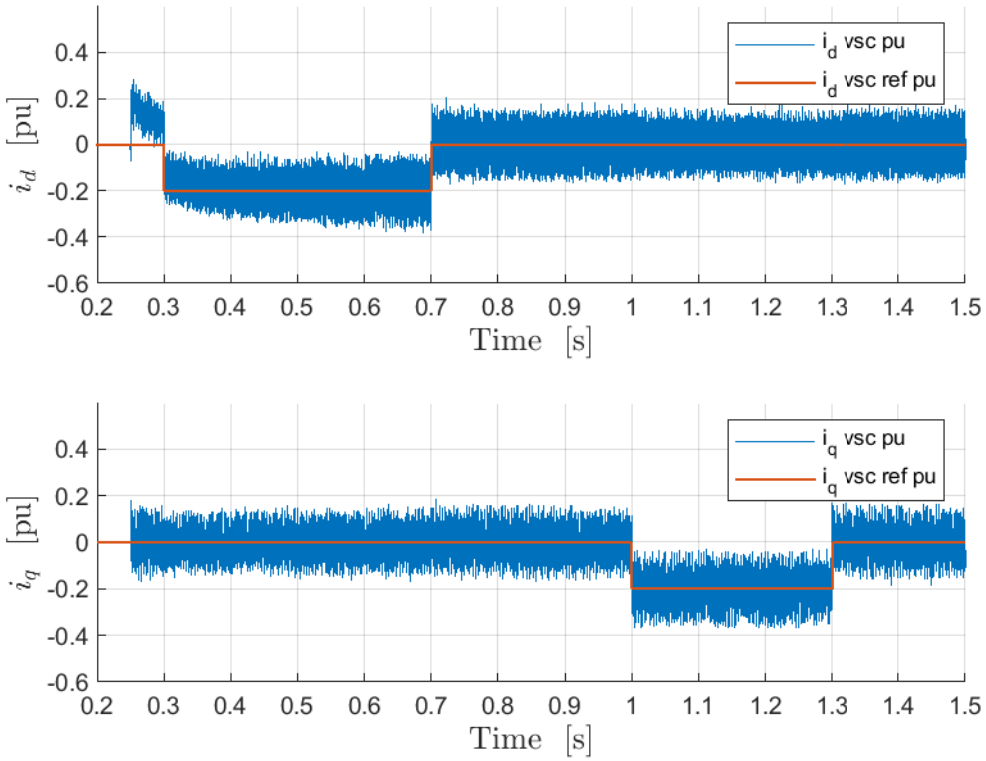

Figure 5.9: STATCOM Inner controller reference tracking.

Timing	Event [pu]
Initially	$v_{pcc,ref} = 0$
t= 0.4 s	$v_{pcc,ref} = 1.05$
t= 0.6 s	$v_{pcc,ref} = 1$
t= 0.8 s	$v_{pcc,ref} = 0.95$
t= 1 s	$v_{pcc,ref} = 1$

Table 5.3: List of events for the outer controller test simulation. Here the variable $v_{pcc,ref}$ is used for V_s^{ref}.

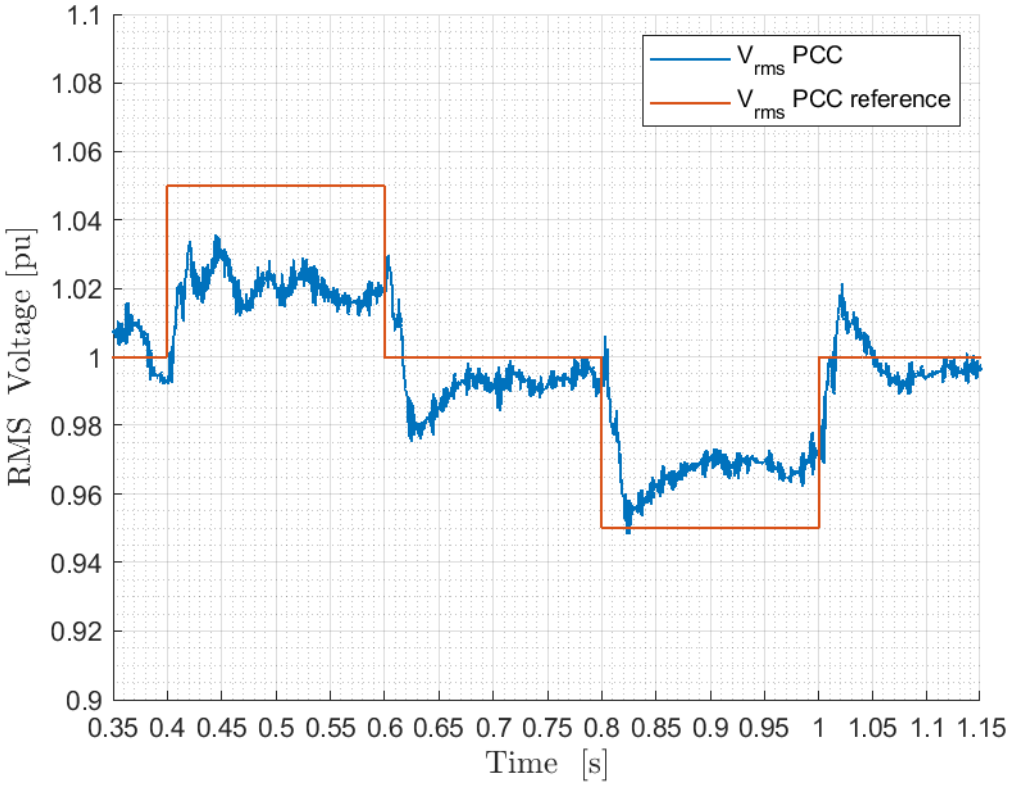

Figure 5.10: STATCOM outer controller reference tracking for V_{PCC}.

Chapter 6

Simulation Results

The corrective action of the MVB and the STATCOM during a motor start and a 3 phase fault are analyzed in this chapter and compared for the two described network systems. In the motor start event, the 12 kVA squirrel cage motor is started at 0.8 seconds and the response of the system as well as the starting time of the motor with the different devices are monitored.

6.1 Test System

Motor Start

The impact of the motor start on the voltage profile at the busbar of *Load2* is assessed. The following list of events considered and simulated are presented in Table 6.1 depending on the technology used to improve the voltage.

MVB		**STATCOM**	
Timing	Event	Timing	Event
t=0 s	Transient load flow	t=0 s	Transient Load flow
t=0.8 s	Breaker of the motor is closed	t=0.05 s	Breaker of STATCOM is closed
		t=0.05 s	Activation STATCOM outer controller
		t=0.8 s	Breaker of the motor is closed

Table 6.1: List of events during the motor start simulation.

As observed in Figure 6.1, the voltage dip during the first instant of the motor start is not the same with or without the presence of the of MVB. Indeed, the dip reaches 0.8 pu in the presence of the MVB while it reaches 0.75 pu without its action. Then, it takes 50 ms to react to the voltage dip and after 200 ms the voltage is brought back to nominal value with the MVB control action. Otherwise, the voltage would remain around 0.77 pu for 1 second before converging towards 0.94 pu after the motor has reached its nominal speed.

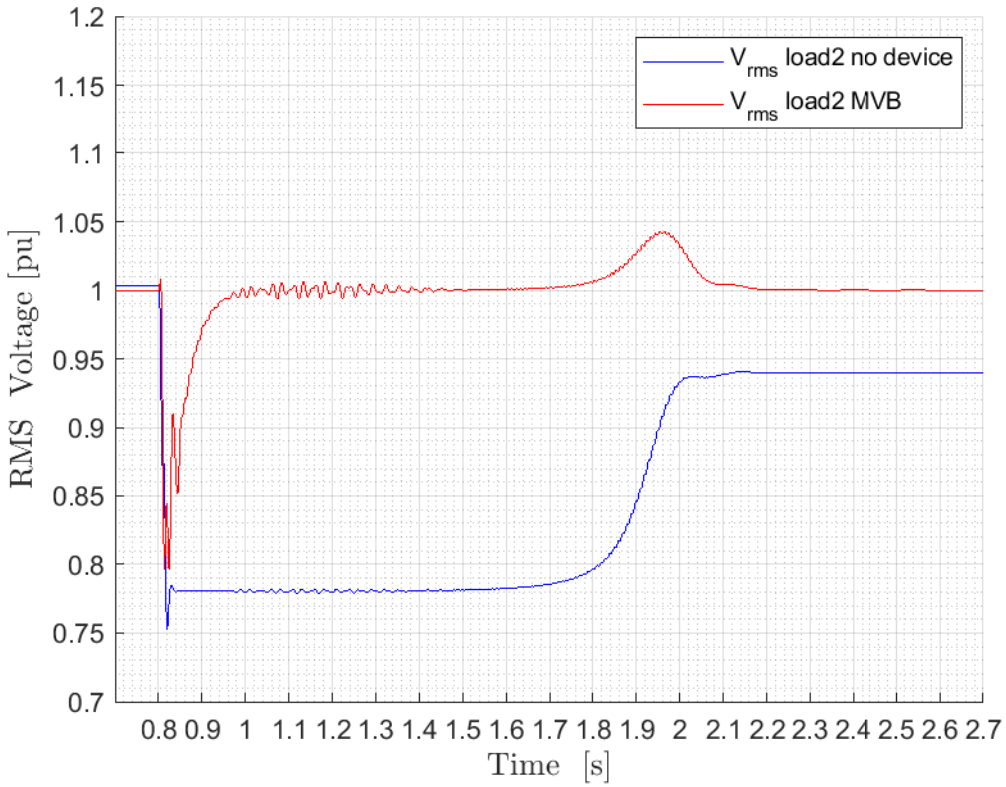

Figure 6.1: Voltage profile during motor start at busbar of load 2 with and without MVB.

It is noticed that some oscillations are present between 1 and 1.5 seconds. These oscillation are due to the oscillating electromagnetic torque created by the induction machine.

In the case of the STATCOM connected to the main bus, one can observe in Figure 6.2 a voltage dip down to 0.8 pu when the motor is started. Then, the STATCOM injects reactive power to stabilize the voltage around 0.95 pu. When the motor has reached nominal speed, there is a slight overshoot up to 1.1 pu before reaching steady state nominal value 1 pu. This overshoot is due to the sudden decrease of the reactive power absorbed by the motor.

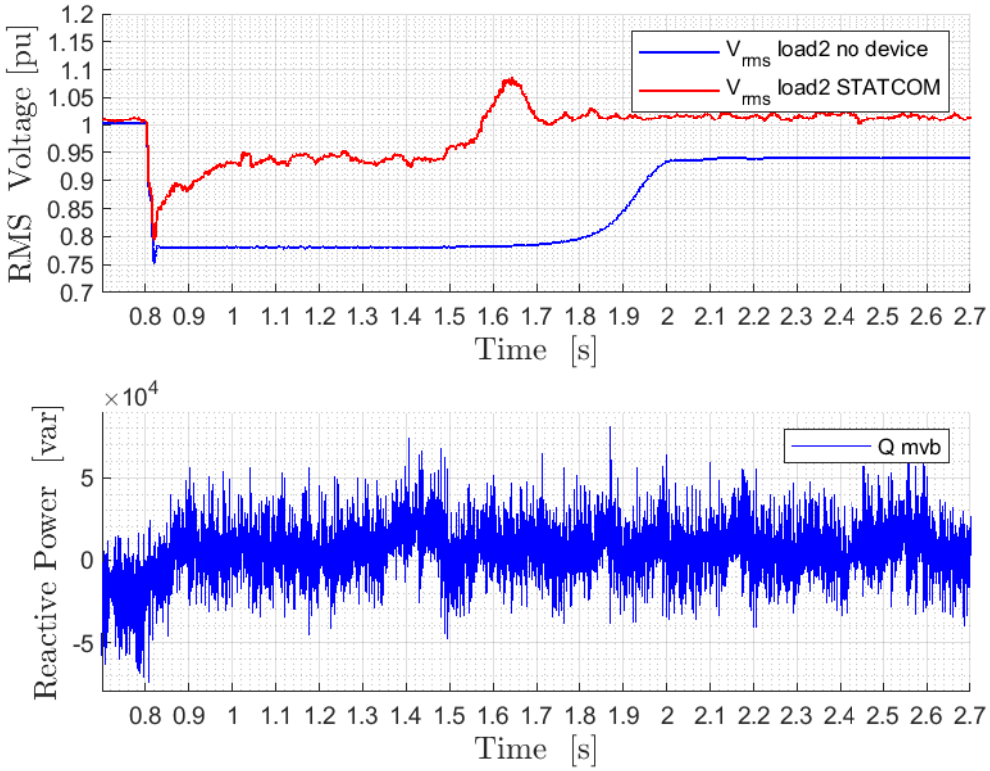

Figure 6.2: Voltage profile during motor start at busbar of load 2 with and without STATCOM. The upper figure shows the voltage profile while the lower figure shows the reactive power injection by the STATCOM.

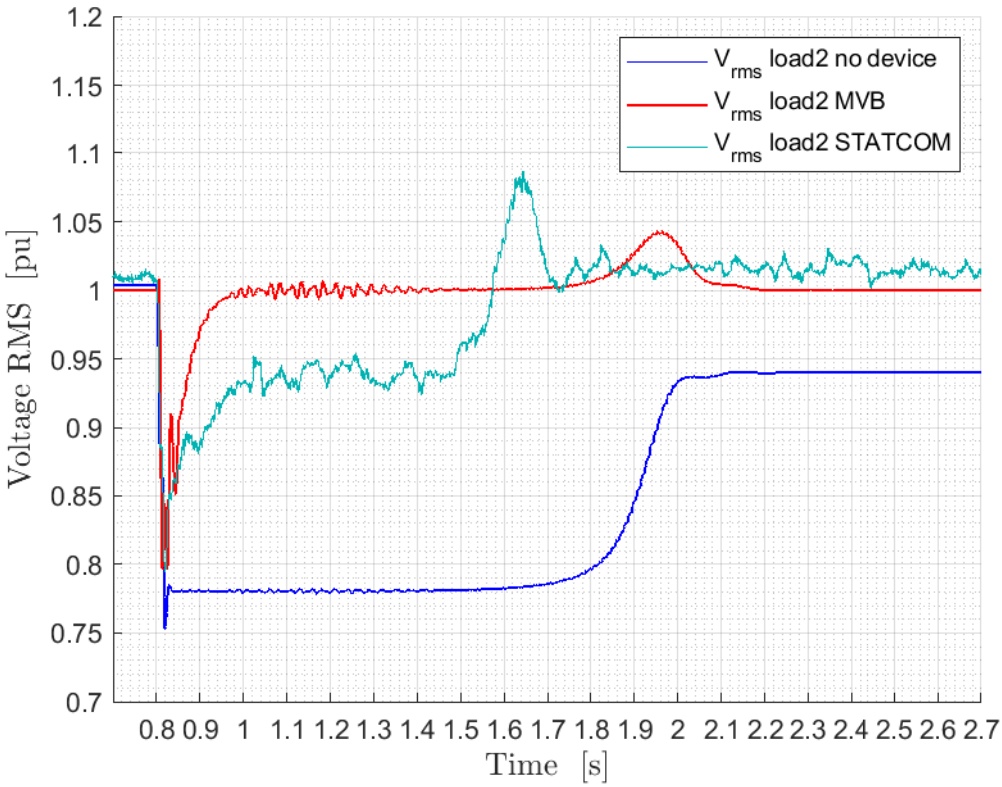

Figure 6.3: Transient evolution of bus B_{Load2} voltage during the motor start of the Test system. Each curve corresponds respectively to the connection of the MVB, the STATCOM or no device to the grid.

The comparison between the MVB and the STATCOM in term of voltage regulation during the motor start is represented in Figure 6.3. One can observe that the MVB is able to restore the nominal voltage of *Load2* significantly faster than the STATCOM. Furthermore, the overshoot at the end of the motor start is smaller for the MVB. It can also be notice that the STATCOM voltage overshoot appears 400 ms before the MVB voltage overshoot.

Comparing the rotor speed evolution of the motor, one can see in Figure 6.4 that in the case of the STATCOM, the nominal value is reached faster than with the MVB. This is due to the higher value reached by the electromagnetic torque in the case of the STATCOM connection because the stator voltage remains close to the nominal value as depicted in Figure 6.5.

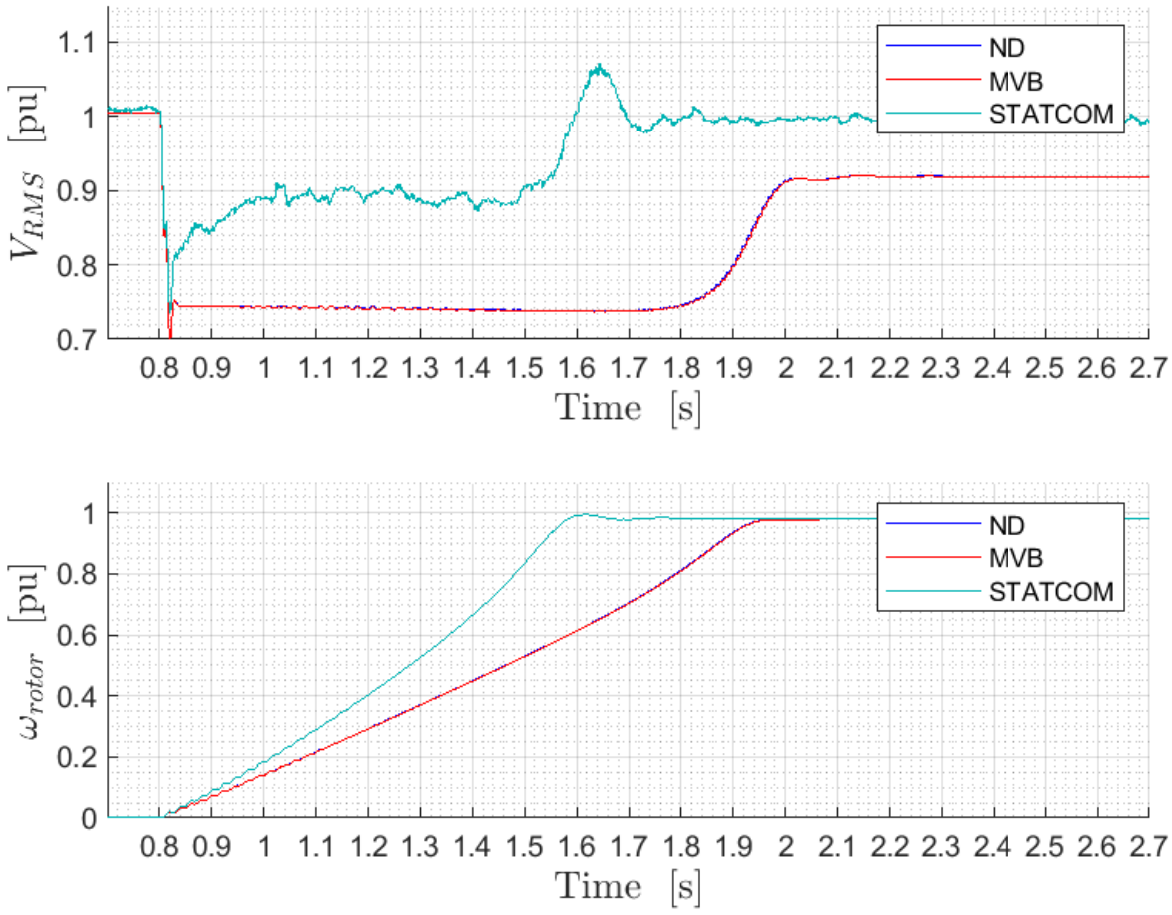

Figure 6.4: The upper and lower plots show respectively the rms voltage of bus B_{Load2} and the mechanical rotor speed when the different devices are connected to the grid. Both voltage and speed evolution for the ND and the MVB case are the merged together.

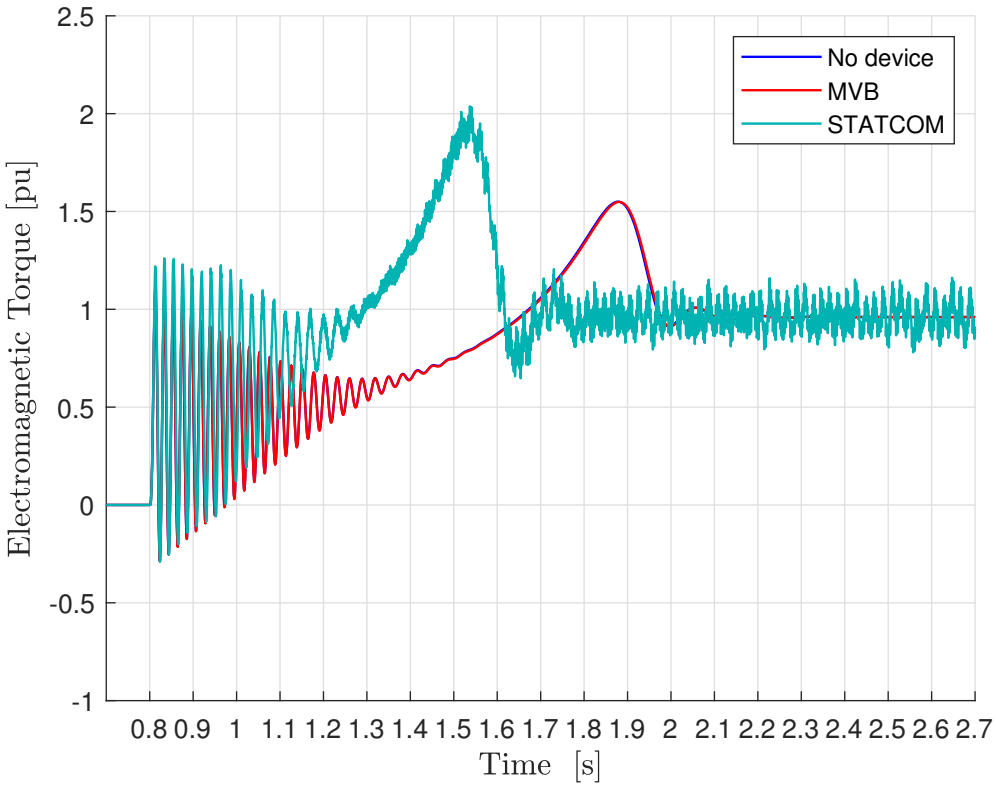

Figure 6.5: Evolution of the electromagnetic torque during the motor start when no device, the MVB and the STATCOM are connected to the main bus (B_{Load2}) of the Test system.

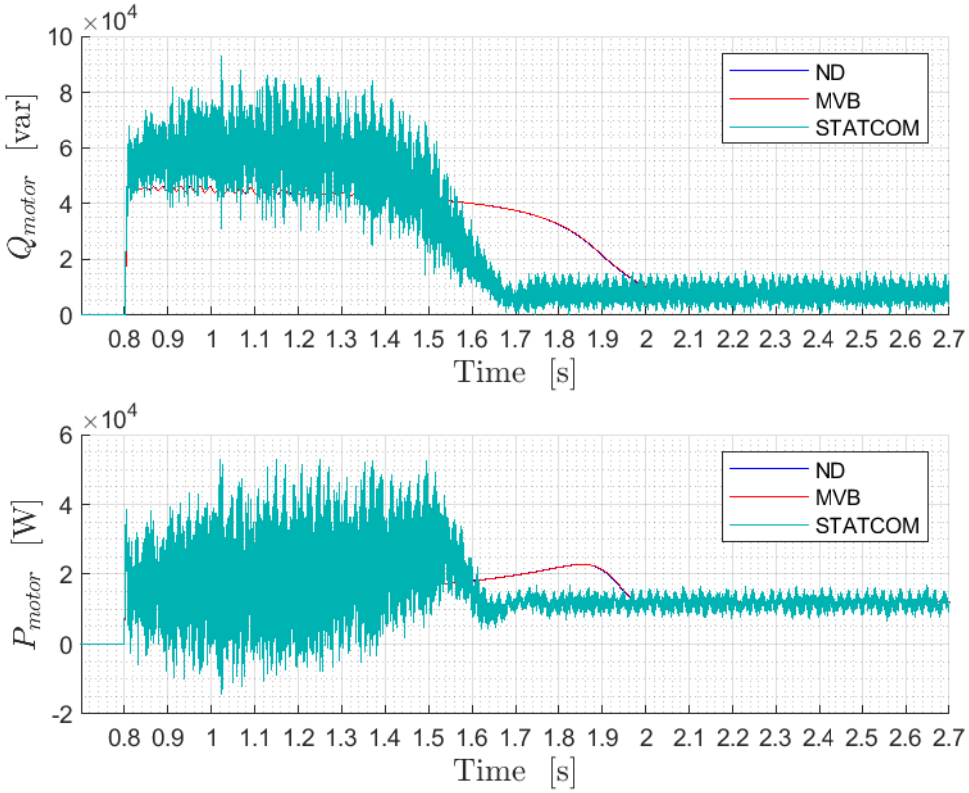

Figure 6.6: The upper and lower plot show respectively the evolution of the reactive and the active power drawn by the motor during its start for the different the different compensation solutions.

Looking at the active and reactive power drawn by the motor during its start, one can see in Figure 6.6 a higher reactive power consumption when the STATCOM is connected to the main bus. Furthermore, the presence of the MVB does not have any influence neither on the reactive nor on the active power consumption compared to the original scenario where none of the device are used.

The active and reactive power consumed by the motor when the STATCOM is connected to the grid present large oscillation as it observed in Figure 6.6. It is noticed that the amplitude of these oscillations is less important when the active and reactive power consumed by the motor, decrease.

Short Circuit

The second event that has been tested on the Test system is a 3 phase to ground fault on the feeder of *Load*. The fault is cleared after 100 ms by opening the circuit breaker of B_{Load}. The list of event used during the simulation is shown in Table 6.2. Since the fault is assumed not 'bolt', the voltage at the busbar B_{Load} will decrease considerably but it will not reach 0 pu due to the presence of the faulted and neutral resistance.

MVB		**STATCOM**	
Timing	Event	Timing	Event
t=0 s	Transient load flow	t=0 s	Transient Load flow
t=0.6 s	Fault on B_{Load}	t=0.2 s	Breaker of STATCOM is closed
t=0.7 s	Breaker of open	t=0.2 s	Activation STATCOM outer controller
		t=0.6 s	Fault on B_{Load}
		t=0.7 s	Breaker open

Table 6.2: List of events during the short circuit simulation.

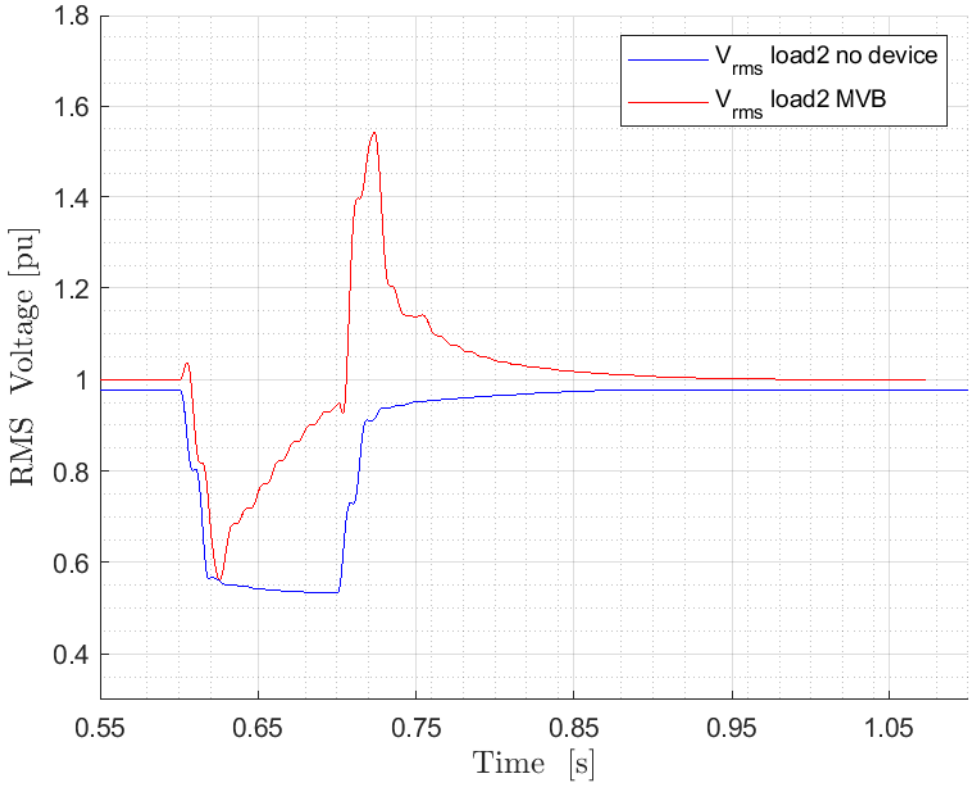

Figure 6.7: Voltage profile at busbar B_{Load2} during the short circuit on busbar B_{Load} with and without MVB.

The voltage dip during the fault when the MVB is connected to busbar B_{Load} is depicted in Figure 6.7. One can notice that the voltage dip reaches 0.5 pu even in the presence of the MVB. Then, the voltage decreases slightly during the next 100 ms when no device is connected while it increases gradually under the MVB controller actions. Once the fault is cleared, the voltage settles back to the pre-fault value in the absence of the MVB while in its presence, the voltage undergoes a large overshoot. This overshoot is due to the topological structure of the MVB. Indeed, since the MVB is connected in serie and because the output voltage is regulated on the basis of the input voltage, the latter has an direct impact on the output voltage.

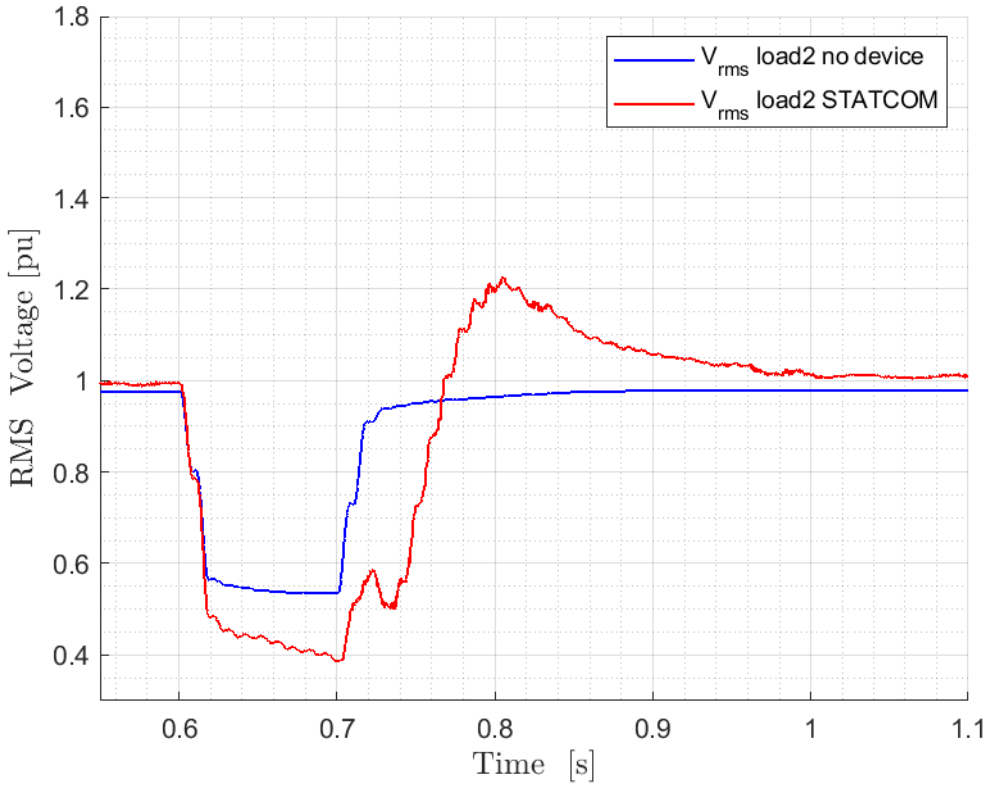

Figure 6.8: Voltage profile at busbar B_{Load} during short circuit on busbar B_{Load} with and without STATCOM.

The evolution of the voltage at the main bus with and without the presence of the STATCOM during the fault is depicted in Figure 6.8. One can see that at the first instant after the fault has occurred, the voltage falls down slightly deeper for the STATCOM scenario than without any device. Although the voltage decreases slightly when no device is connected to the bus, it decreases even faster when the STATCOM is present. Then, at 0.7 s, the voltage is restored due to the clearing of the fault. It is worth noting that the voltage goes back into the admissible range [0.95,1.05] only after 300 ms when the STATCOM is connected. This is due to the STATCOM controller that has injected during the fault a large amount of reactive

power which is unnecessary once the fault is cleared.

In order to compare the qualitative performance of the MVB with the STATCOM, the voltage evolutions during the short circuit for each devices connected are plot and represent in Figure 6.9. One can first observe that the STATCOM decrease the voltage dip. During the fault period, thanks to the serie voltage injection, the voltage dips on the load side is reduced when it is not the case with the STATCOM. Finally, after the fault is cleared, both device increases their controlled voltage with an unadmissible overshoot (¿1.15 pu). However, the overshoot of the STATCOM is smaller than the one of the MVB by 0.5 pu. Both depends on the speed of the controllers.

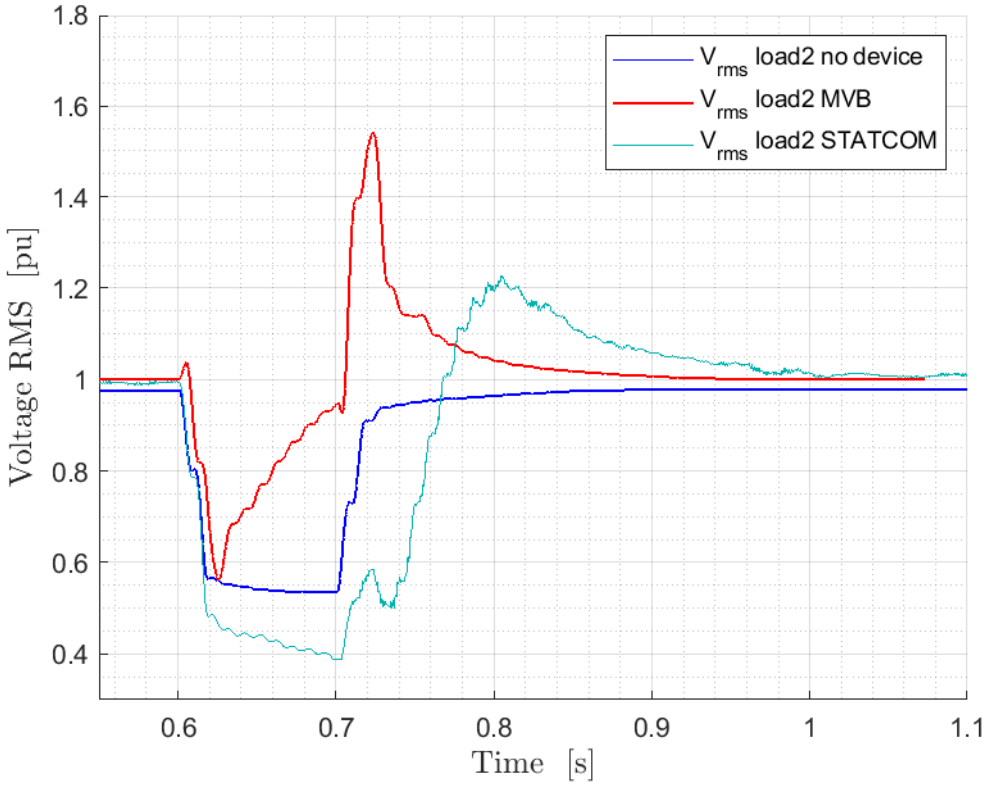

Figure 6.9: Comparison of the voltage profile during the short circuit on busbar B_{Load} without device, with MVB and with STATCOM.

6.2 Case System

The same simulations as with the Test system are conducted in the Case system. In order to model the motor start, a squirrel cage induction machine of 12 kVA is connected to the the load $LB5a$. The compensation device will be placed between bus B1t and bus BA1. Furthermore, the voltages of bus B1t and BA1 are analysed. The same list of events (motor start and short circuit) as in the Test grid simulations are considered.

Motor Start

The voltage are depicted in Figure 6.10. It can be observed that when the motor is started, it created a depressed voltage below 0.9 pu. If no device is connected, the voltage remains below 0.9 pu for 900 ms before increasing and reaching the steady state value of 0.97 (i.e. the duration of the motor start transient).

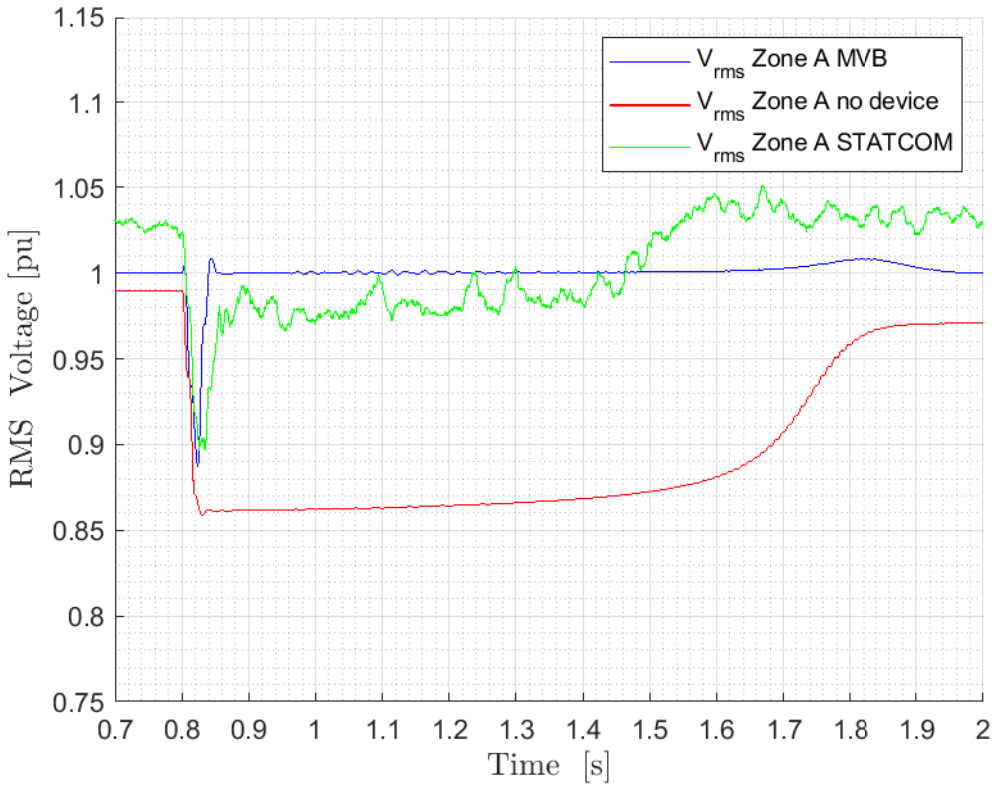

Figure 6.10: The voltage dip on bus $BA1$ during the motor start is represented in three cases: with MVB, without device and with STATCOM.

When the STATCOM or the MVB are connected to the grid, the voltage is brought back into the admissible range after 50 ms for the STATCOM and after 20 ms for the MVB. Finally,

when the motor has reached its nominal rotor speed, both devices undergoes an overshoot due to the reactive power consumption drop by the motor.

Short Circuit

The short circuit is simulated at 0.6 s during 100 ms. Figure 6.11 indicates a voltage dip of 20%. This happens in the case where the STATCOM or no device is connected to grid. On the other hand, when the MVB is connected to grid, the voltage dip is mitigated and reaches 0.87 pu. During the fault, only the MVB is able to the recover the nominal voltage level at his right side while the STATCOM is only able to bring the voltage in the admissible range. After the fault is cleared, the steady voltage is recovered as expected when no device is connected to the grid while a large overshoot is observed when the STATCOM or the MVB is connected.

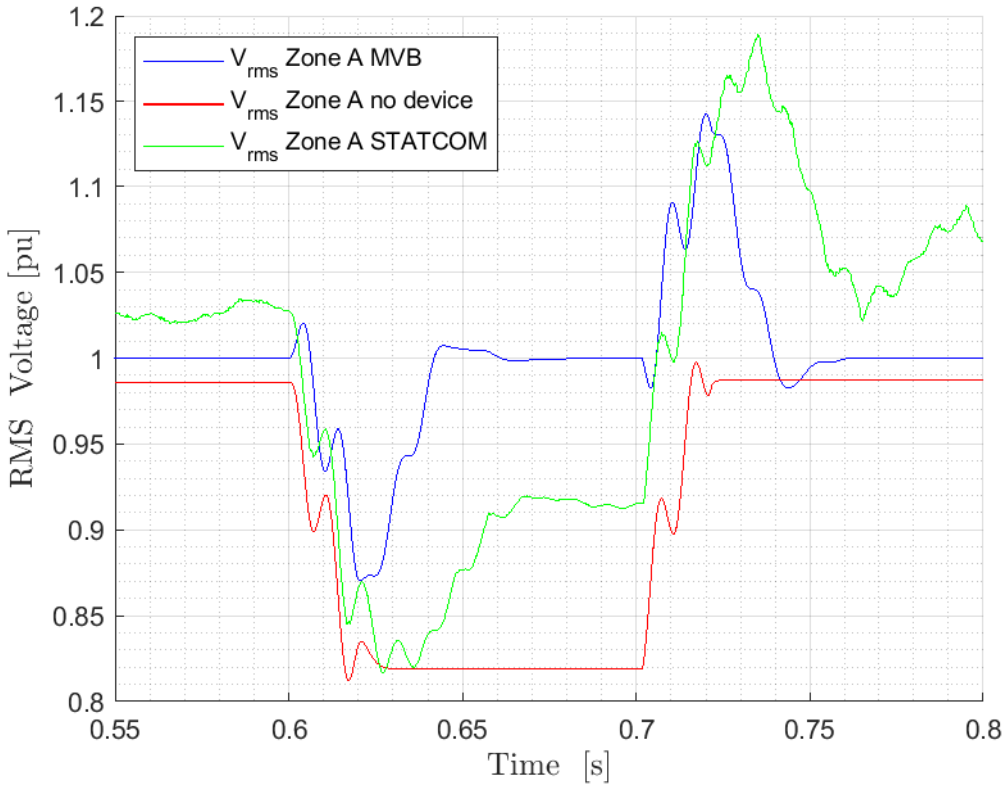

Figure 6.11: Voltage evolution during the short circuit when the different device (MVB, STATCOM and no device) are connected to the grid.

Conclusion

The scope of the thesis was to analyze the voltage profile in low voltage distribution network and implement different device to mitigate the voltage dip that the distribution grid experiences during motor starts and short circuit events. In that frame, the topology and the parameters data of the low voltage distribution network were received from the local grid company TrondEnergy^{AS} and a model of the electrical grid has been reproduced within the $MATLAB$®/ $Simscape$® environment. Then, a power flow computations was run with an independent software MATPOWER and the voltage magnitude of the grid were compared to the one of the $Simscape$® steady state results. Although the power flow results obtained with $Simscape$® did not exactly match the power flow results of the grid company and of the MATPOWER software, the tendency of the local voltage was respected. It is noted that due to the very long simulation times, the distribution system model had to be to some extent simplified.

In order to model the voltage dip, a 12 kVA squirrel cage induction motor has been implemented using the built-in model provided by the $Simscape$® toolbox. Then, the cause of the voltage dip has been enlightened by analyzing the active and reactive power consumption of the motor during its start. Moreover, these two powers appeared to be used for the build-up of the electromagnetic torque. The latter allowing the rotor speed to increase with large oscillation and finally overcoming the friction and load torque. Thus, reactive compensation during the motor start allows the motor to start faster and doing so, it reduce the voltage dips duration.

The two solutions that were compared, operate on rather different voltage compensation principles: the MVB compensates the secondary side voltage by adding a voltage in series when the STATCOM belongs to the shunt compensation solutions family. Also, although both solutions include fast electronic regulating controller, the MVB core principle is to adapt the voltage added in series thanks a 'virtually built air gap' in the magnetic core while the STATCOM injects a reactive current to control the voltage at a given location in the grid.

The developed model and expected benefits of both solutions were first tested on a simple system before tested into the larger system representing a portion of the TrondEnergy distribution company. Achieved results indicates that in line with their operating principle, the MVB technology impacts positively the voltages downstream the MVB while the STATCOM controls its terminal voltage and hence the voltage profile in its close vicinity by injecting

a reactive current and therefore Mvar in the system. Moreover, the short circuit simulation with the MVB has revealed the limitation of this technology since the regulation is a highly dependent of the voltage magnitude upside the device.

Another significant difference between the two solutions is that for medium amplitude voltage dips, the MBV is intrinsically easier if not straightforward to deploy and tune as it is composed by only one feedback loop controlling the secondary voltage. On the contrary, the STATCOM operation relies on two hierarchical loops (inner and outer) and a PLL to maintain the quadrature of the injected reactive current. Also, due to the 2-level topology assumed for the STATCOM, rather high level of noise was observed. In order to reduce this noise, it would have required to add a dedicated filter downstream the series R_f-L_f part of the STATCOM.

6.3 Futher work

This thesis has investigated the use of two different technologies which proposes corrective action towards the voltage quality. However, one could also search for solutions to tackle the problem directly at the source. For instance, the voltage dips duration could be reduced by starting the motors faster with different technologies such as variable frequency converter and soft starter. The magnetic voltage booster technology could also be compared with shunt connected rotating machine (asynchronous, synchronous and flywheel). These latter are able to provide short circuit capacity during fault event.

On the corrective actions studied in this thesis, one can improve the accuracy of the analysis by removing several assumptions made with the modelling of the different devices. Concerning the Magnetic voltage booster, one can take into account the modelling of the rectifier by including the power electronic part as well as the dynamic of the Magnetic Controllable Inductor. For instance, the Jiles–Atherton model[19] can be used to model the magnetic behaviour of the variable inductance. In the STATCOM modelling, the ideal switches of the VSC can be replaced by IGBT's and several filters bank can be added at the point of common coupling to remove the non-negligible harmonics and thus improving the voltage quality.

Another point that can be investigated is the determination of the optimal location of these voltage regulation devices as well as a cost analysis between the two technologies.

Appendix A

Grid Parameters

Appendix A includes all the parameters of the transmission line as well as the nominal power (active and reactive) that have been used during the transient simulation of the different *Simulink/Simscape* models.

A.1 Cable Data

The numerical value of the Π equivalent model for the different cable types are given in Table A.1[20][21].

Parameter	R	X	$C_{line-line}$	$C_{line-ground}$
Units	$[\frac{\Omega}{km}]$	$[\frac{\Omega}{km}]$	$[\frac{nF}{km}]$	$[\frac{nF}{km}]$
AL 1X25	0.717	0.345	4.3	10.72
AL 1X50	0.256	0.312	4.48	11.91
EX 1X25	1.2	0.082	0.28	0.55
EX 1X50	0.641	0.077	0.41	0.8
EX 1X95	0.32	0.076	0.52	1.09
PFSP 1X3X25 AL	1.2	0.082	0.42	0.82
PFSP 1X3X50 AL	0.641	0.079	0.53	1.08
TFXP 1X4X95 AL	0.32	0.075	0.57	1.1
TFXP JETNET 1X4X50	0.641	0.079	0.53	1.08
TFLP 1X3X95 AL	0.32	0.075	0.57	1.1

Table A.1: Parameter values of the cable used in the network.

A.2 Case Network Data

Branch Type

The cable type and lengths of each branch showed in Table A.2.

Line	Length [km]	Line Type
B1t_BA1	0.85	TFXP_1X4X95_AL
BA1_BA2	0.252	EX_1X95
BA2_BA3a	0.21	EX_1X25
BA2_BA3b	0.12	EX_1X25
BA2_BA3c	0.52	EX_1X95
BA3c_BA4a	0.22	PFSP_1X3X25_AL
BA3c_BA4b	0.60	EX_1X95
BA4b_BA5	0.120	EX_1X95
BA5_BA6	0.134	EX_1X50
B1t_BB1	0.85	TFXP_1X4X95_AL
BB1_BB2	0.664	EX_1X95
BB2_BB3a	0.70	EX_1X50
BB2_BB3b	0.194	EX_1X50
BB3a_BB4	0.3	TFLP_1X3X95_AL
BB4_BB5a	0.21	PFSP_1X3X25_AL
BB4_BB5b	0.68	PFSP_1X3X50_AL
B1t_BC1	0.85	TFXP_1X4X95_AL
BC1_BC2	0.54	EX_1X95
BC2_BC3	0.130	AL_1X50
BC3_BC4	0.178	AL_1X25
BC4_BC5a	0.27	EX_1X25
BC4_BC5b	0.77	AL_1X25
BC5a_BC6a	0.21	PFSP_1X3X25_AL
BC5b_BC6b	0.37	EX_1X25

Table A.2: Cable type and length of each transmission line.

Power flow initial DATA

Load Name	Nominal Voltage [V]	Nominal P [kW]	Nominal Q [kVar]
LA3a	230	3.7	0.75
LA3b	230	3.7	0.75
LA4a	230	0.394	0.08
LA6	230	6.516	1.323
LB3b	230	0.1	0.1
LB5a	230	6.141	1.247
LB5b	230	0.1	0.1
LC6a	230	2.186	0.444
LC6b	230	0.095	0.019

Table A.3: Load flow data of the Case network.

A.3 Test Network Data

Line Type

Line	Length [km]	Line Type
BLV_BLoad	2	TFXP_1X4X95_AL
BLoad_BMotor	1	TFXP_1X4X95_AL

Table A.4: Line parameters of the Test network.

Power flow initial Data

Load Name	Nominal Voltage [V]	Nominal P [kW]	Nominal Q [kVar]
Load	230	0.5	0
Load2	230	0.5	0
Motor	230	6	3.8

Table A.5: Load flow data of the test network.

Appendix B

MVB & STATCOM Parameters

B.1 Characteristic Data of a MVB device

The maximum load connected to the main grid consumes in steady state around 8 kVA. The rating of the MVB device is therefore chosen to be 10 kVA. Table B.1 shows the relevant useful electrical characteristics[22] of a 10 kVA MVB.

Ratings [kVA]	**10**
Frequency [Hz]	50
Nominal phase to ground voltage [V]	230
Nominal Load [kVA]	10
Nominal current [A]	25
Voltage boost [%]	0,...,+17
Dynamic time response [ms]	150

Table B.1: Electrical characteristic of a 10 kVA MBV device.

B.2 STATCOM in Per Unit

The base value of the STATCOM parameters are represented in Table B.2. These are computed using the following triplet of base value:

$$S_B = 100 \text{ kVA} \qquad V_B = 230 \text{ V} \qquad f_B = 50 \text{ Hz} \tag{B.1}$$

Parameters	Expression	Value	Unit
ω_B			$\frac{\text{rad}}{\text{s}}$
$S_{AC,B}$	S_B	100	kVA
$V_{AC,B}$	$\sqrt{2}V_B$	325.27	V
$I_{AC,B}$	$\frac{2S_B}{3V_{AC_B}}$	204.96	A
$Z_{AC,B}$	$\frac{V_{AC,B}}{I_{AC,B}}$	1.587	Ω
$R_{AC,B}$	$Z_{AC,B}$	1.587	Ω
$L_{AC,B}$	$\frac{Z_{AC,B}}{\omega_B}$	0.005	Ω
$C_{AC,B}$	$\frac{1}{\omega_B Z_{AC,B}}$	0.002	F
$S_{DC,B}$	$S_{AC,B}$	100	kVA
$V_{DC,B}$	$2V_{AC,B}$	650.54	V
$I_{DC,B}$	$\frac{S_{DC,B}}{V_{DC,B}}$	153.72	A
$Z_{DC,B}$	$\frac{V_{DC,B}}{I_{DC,B}}$	4.23	Ω
$R_{DC,B}$	$\frac{8}{3}L_{AC,B}$	4.23	Ω
$C_{DC,B}$	$\frac{3}{8}C_{AC,B}$	0.0075	F

Table B.2: Base value used for the STATCOM equations in per unit.

B.3 Modulus Optimum Tuning

The value of the inner PI controller gains k_p^{in} and k_i^{in} are obtained by applying the Modulus Optimum and Lead compensation method[23]. This tuning technique is based on a general control system structure depicted in Figure B.1 where the gains of the PI controller k_p and k_i are made dependent of the plant transfer function parameters and where Y_{ref}, Y, D and U designate respectively the signal reference, the control signal, some disturbance and the input signal.

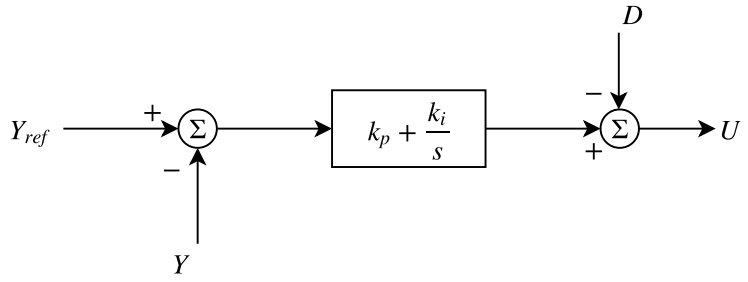

Figure B.1: General control structure suitable for Modulus Optimum and lead compensation[23].

Assuming a general plant transfer function $H_{plant}(s)$ of the second order degree given by Equation (B.2).

$$H_{plant}(s) = \frac{k}{(1+sT)(1+sT_f)} \tag{B.2}$$

the general expression of k_p and k_i are given by Equation (B.3a-b)

$$k_p = \frac{T}{2T_f\ k} \tag{B.3a}$$

$$k_i = \frac{k_p}{T} \tag{B.3b}$$

Since the transfer functions of the VSC and of the PI controller are is given by Equation (B.4):

$$H_{VSC}(s) = \frac{1}{R_f} \frac{1}{1 + s\left(\frac{L'_f}{R_f}\right)} \frac{1}{1 + sT_f} \tag{B.4a}$$

$$H^{in}_{PI}(s) = k^{in}_p + \frac{k^{in}_i}{s}, \tag{B.4b}$$

By identification with Equation (B.3), the expressions of the gains k^{in}_p and k^{in}_i are obtained :

$$k^{in}_p = \frac{L'_f}{2T_f} \tag{B.5a}$$

$$k^{in}_i = \frac{R_f}{2T_f} \tag{B.5b}$$

where $k = \frac{1}{R_f}$, $L'_f = \frac{L_f}{\omega_b}$ and $T = \frac{L'_f}{R_f}$.

Appendix C

Reference Frame Transformation

C.1 $\alpha\beta$ Reference Frame

Three phase variable such as voltage or current can be condensed into one rotating space vector. In the sequel we will use the variable f_a, f_b and f_c to denote this 3 phases variables. Let $\overrightarrow{f}(t)$ be the rotating space phasor depicted in Figure C.1 composed of the oscillating quantities f_a, f_b and f_c. This rotating space phasor rotating at angular speed $\omega(t)$ can be expressed as in Equation (C.1).

$$\overrightarrow{f}(t) = \frac{2}{3}[f_a(t)e^{j0} + f_b(t)e^{j\frac{2\pi}{3}} + f_c(t)e^{j\frac{4\pi}{3}}] \tag{C.1}$$

where f_a, f_b and f_c. are given by Equations. (C.2a-c) and $\hat{f}$ denoted the amplitude of f_k (k=a,b,c)

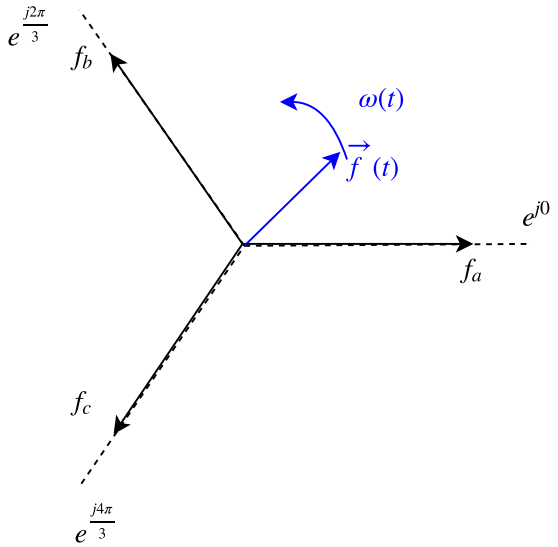

Figure C.1: Diagram of the rotating space phasor .

$$f_a(t) = \hat{f}cos(\omega t + \theta_0) \tag{C.2a}$$

$$f_b(t) = \hat{f}cos(\omega t + \theta_0 + \frac{2\pi}{3}) \tag{C.2b}$$

$$f_c(t) = \hat{f}cos(\omega t + \theta_0 + \frac{4\pi}{3}) \tag{C.2c}$$

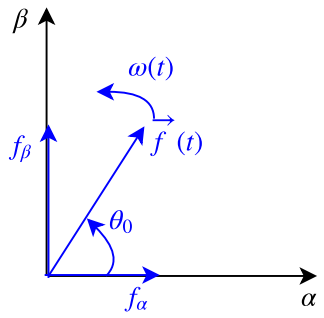

Figure C.2: $\alpha\beta$ reference frame.

In a complex plane as depicted in Figure C.2, $\overrightarrow{f}(t)$ can be represented in phasor notation as

$$\overrightarrow{f}(t) = \hat{f}e^{j\theta_0}e^{j\omega t} = \overline{f}e^{j\omega t} = f_\alpha(t) + jf_\beta(t), \tag{C.3}$$

where $f_\alpha(t)$ and $f_\beta(t)$ are the oscillating component of $\overrightarrow{f}(t)$ projected into a two dimensional static reference frame called $\alpha\beta$.It should be mentioned that the static reference frame $\alpha\beta$ is in fact a $\alpha\beta\gamma$ frame where the γ axis is perpendicular to the $\alpha\beta$ plane but for a balanced 3 phase system, the gamma component is equal to zero and is thus not represented.

The transformation that allows to pass from the abc components to the $\alpha\beta\gamma$ components of $\overrightarrow{f}(t)$ is called the Clarke transformation and is given in Equation (C.4):

$$\begin{bmatrix} f_\alpha \\ f_\beta \end{bmatrix} = \frac{2}{3} \underbrace{\begin{bmatrix} 1 & \frac{-1}{2} & \frac{-1}{2} \\ 0 & \frac{-\sqrt{3}}{2} & \frac{\sqrt{3}}{2} \end{bmatrix}}_{Clark\ transform} \begin{bmatrix} f_a(t) \\ f_b(t) \\ f_c(t) \end{bmatrix} \tag{C.4}$$

C.2 dq Rotating Reference Frame

When it comes to control oscillating signals, it is easier to pass them into constant variable. Therefore, by projecting the space phasor $\overrightarrow{f}(t)$ on a reference frame that rotates, the components of $\overrightarrow{f}(t)$ in this new rotating reference frame can be made time invariant by a proper choice of $\rho(t) = \omega(t) + \theta_0$ in steady state operation. This new rotating reference frame is denoted by dq[1] and the concept is illustrated in Figure C.3.

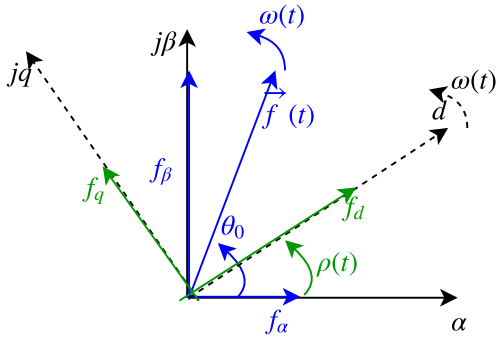

Figure C.3: dq rotating reference frame.

Mathematically, the dq components of $\overrightarrow{f}(t)$ are obtained by removing the oscillatory factor $e^{j\rho t}$ from $\overrightarrow{f}(t)$ in Equation (C.3).

$$f_d + jf_q = \overrightarrow{f}(t)e^{-j\rho(t)} = \hat{f}e^{j\theta_0} \tag{C.5}$$

The transform that allows to pass from the oscillatory abc components to the dq components is called the Park transform and its expression is given by Equation (C.4).

$$\begin{bmatrix} f_d \\ f_q \end{bmatrix} = \frac{2}{3} \underbrace{\begin{bmatrix} cos(\rho(t)) & cos(\rho(t) - \frac{2\pi}{3}) & cos(\rho(t) - \frac{4\pi}{3}) \\ sin(\rho(t)) & sin(\rho(t) - \frac{2\pi}{3}) & sin(\rho(t) - \frac{4\pi}{3}) \end{bmatrix}}_{Park\ transform} \begin{bmatrix} f_a(t) \\ f_b(t) \\ f_c(t) \end{bmatrix} \tag{C.6}$$

[1]Once again, the correct rotating reference frame has 3 components: d, q and 0. Since balanced 3 phase operation is considered, the 0 component is equal to zero and is thus omitted.

Appendix D

MATLAB Scripts And Models

Test Network-Single Line Diagram

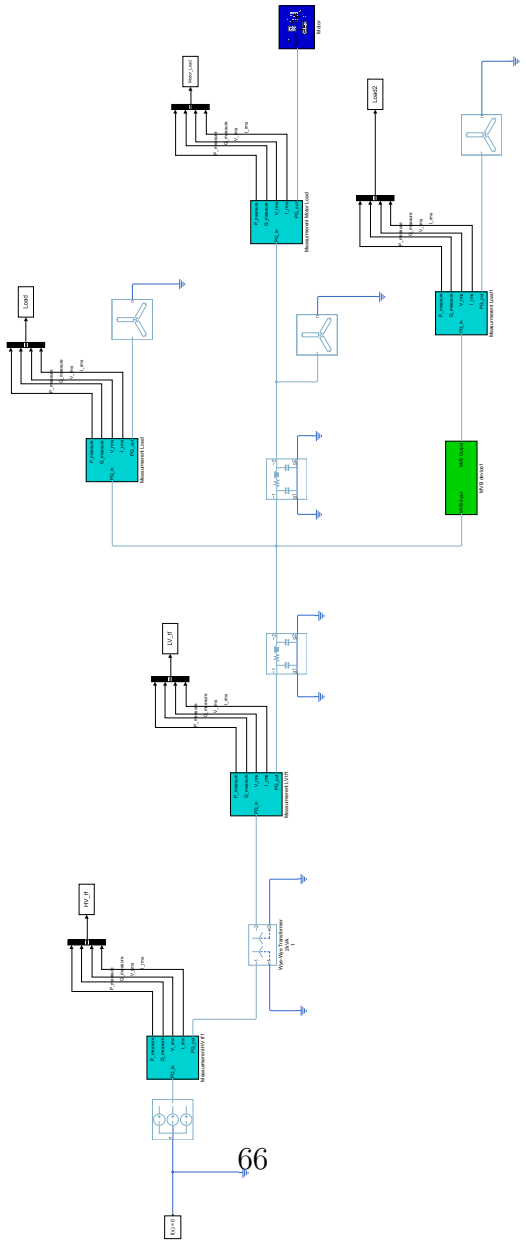

Case Network-Single Line Diagram

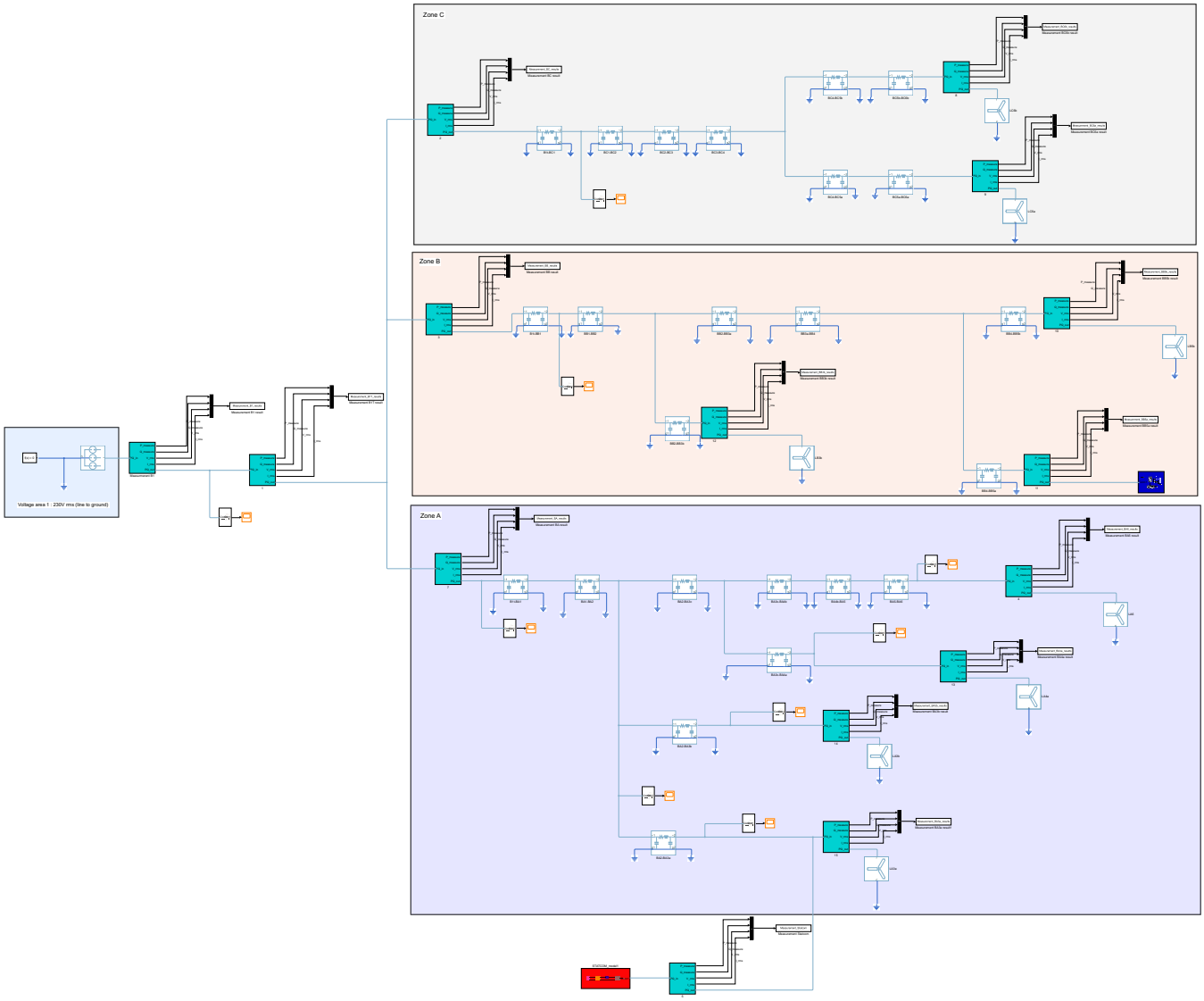

Motor model

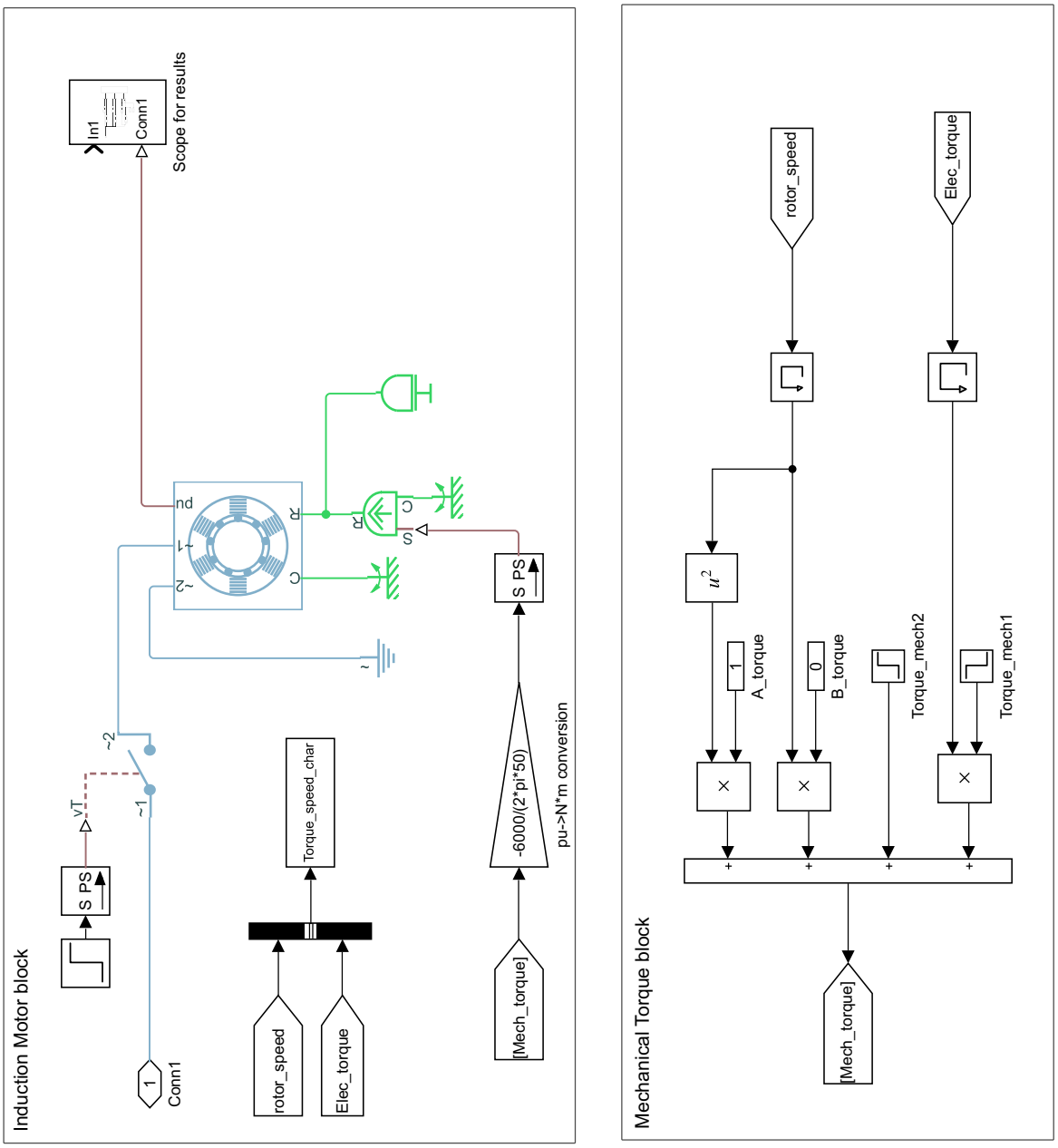
Induction Motor block
In1
Conn1
Scope for results
nd
R
C
S
~1
~2
~2
~1
vT
S PS
1
Conn1
Torque_speed_char
rotor_speed
Elec_torque
-6000/(2*pi*50)
pu->N*m conversion
S PS
[Mech_torque]
Mechanical Torque block
rotor_speed
Elec_torque
u^2
1
A_torque
0
B_torque
Torque_mech2
Torque_mech1
[Mech_torque]

MVB-Model

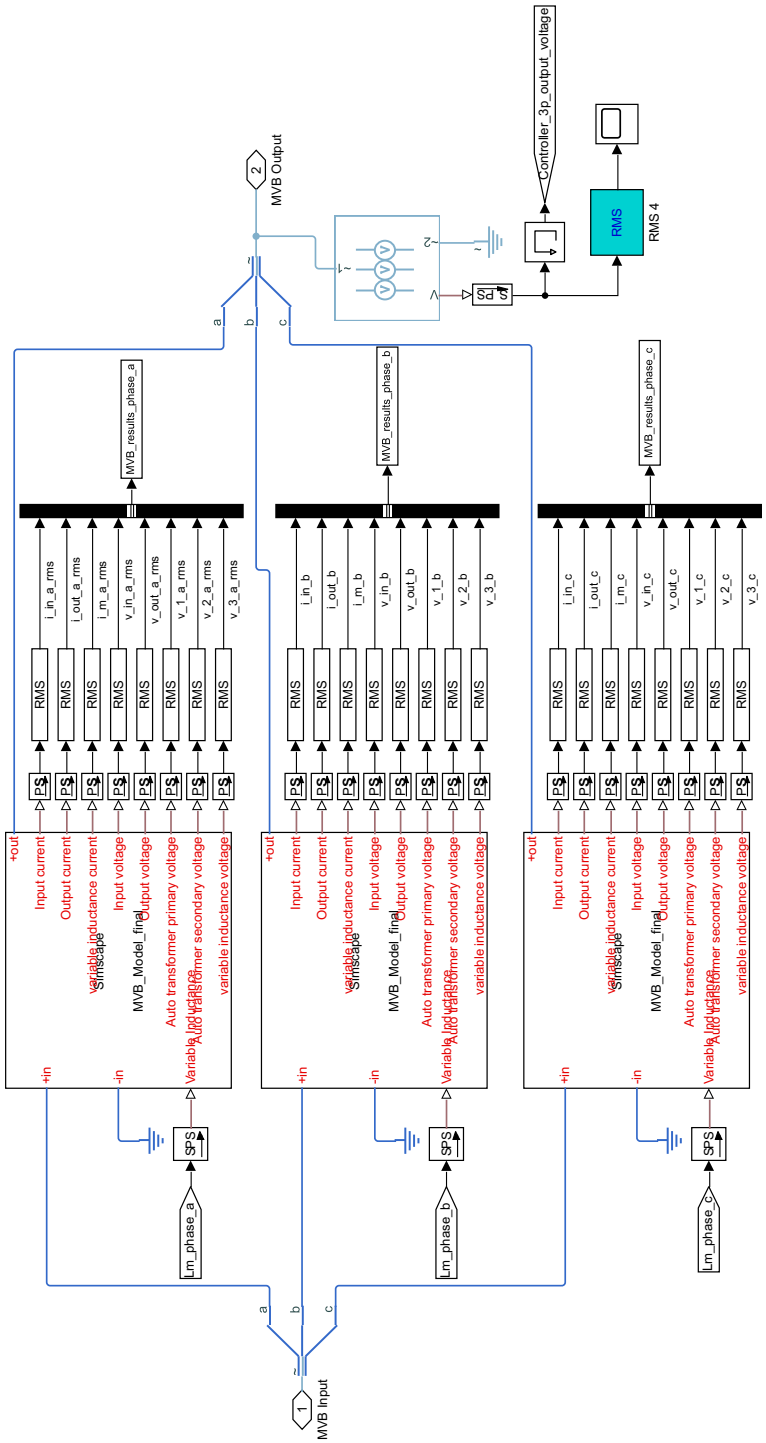
MVB Output
Controller_3p_output_voltage
RMS
RMS 4
MVB_results_phase_a
MVB_results_phase_b
MVB_results_phase_c
i_in_a_rms
i_out_a_rms
i_m_a_rms
v_in_a_rms
v_out_a_rms
v_1_a_rms
v_2_a_rms
v_3_a_rms
i_in_b
i_out_b
i_m_b
v_in_b
v_out_b
v_1_b
v_2_b
v_3_b
i_in_c
i_out_c
i_m_c
v_in_c
v_out_c
v_1_c
v_2_c
v_3_c
RMS
PS
Simscape
MVB_Model_final
Input current
Output current
variable inductance current
Input voltage
Output voltage
Auto transformer primary voltage
Auto transformer secondary voltage
variable inductance voltage
+out
+in
-in
SPS
Lm_phase_a
Lm_phase_b
Lm_phase_c
MVB Input

MVB-Controller

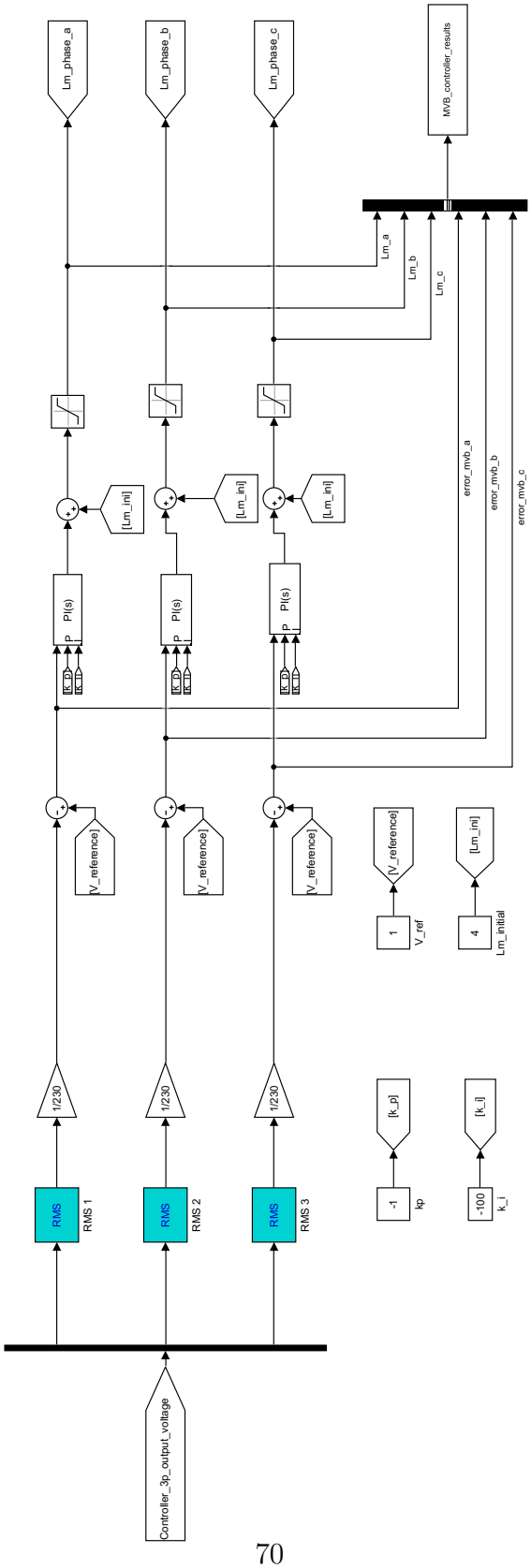

STATCOM-Global Model

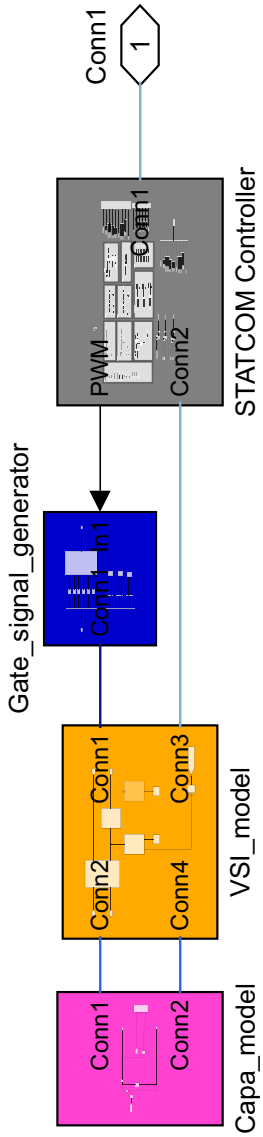

STATCOM-Inverter Model

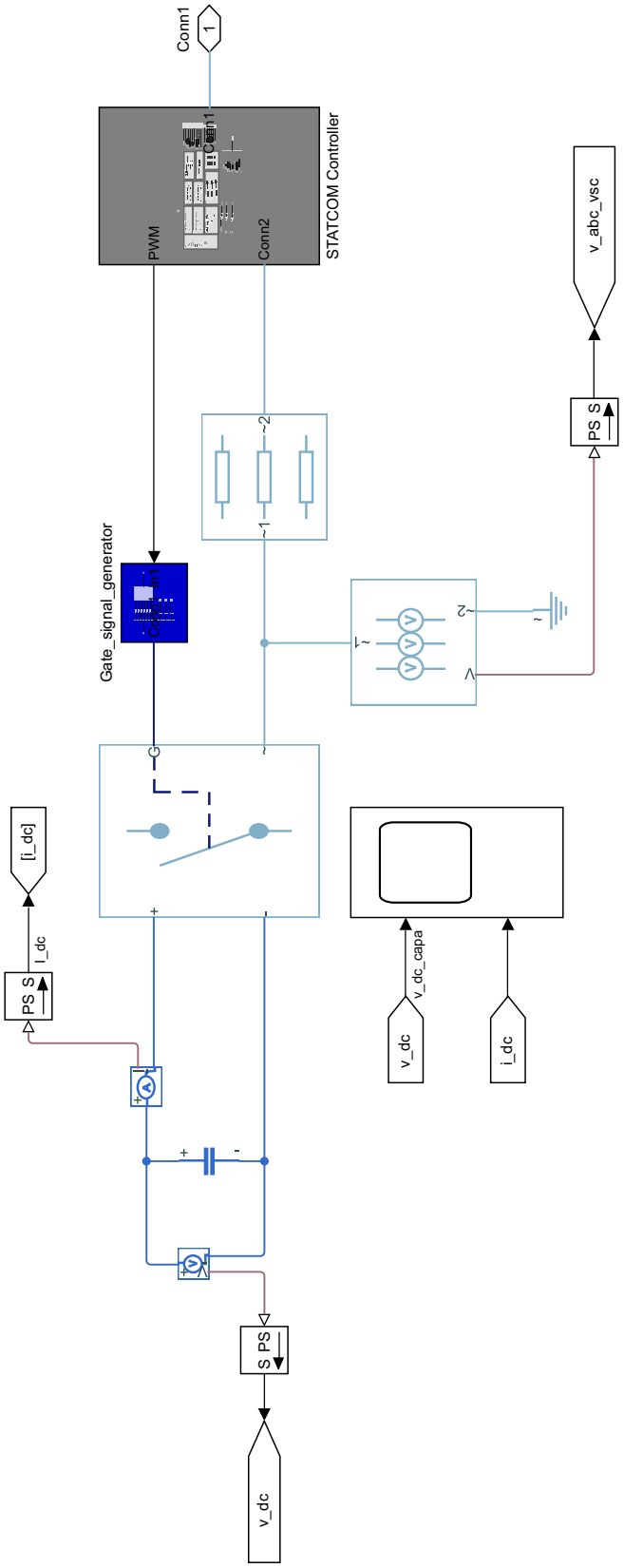

STATCOM-Sensor-PLL-PWM Model

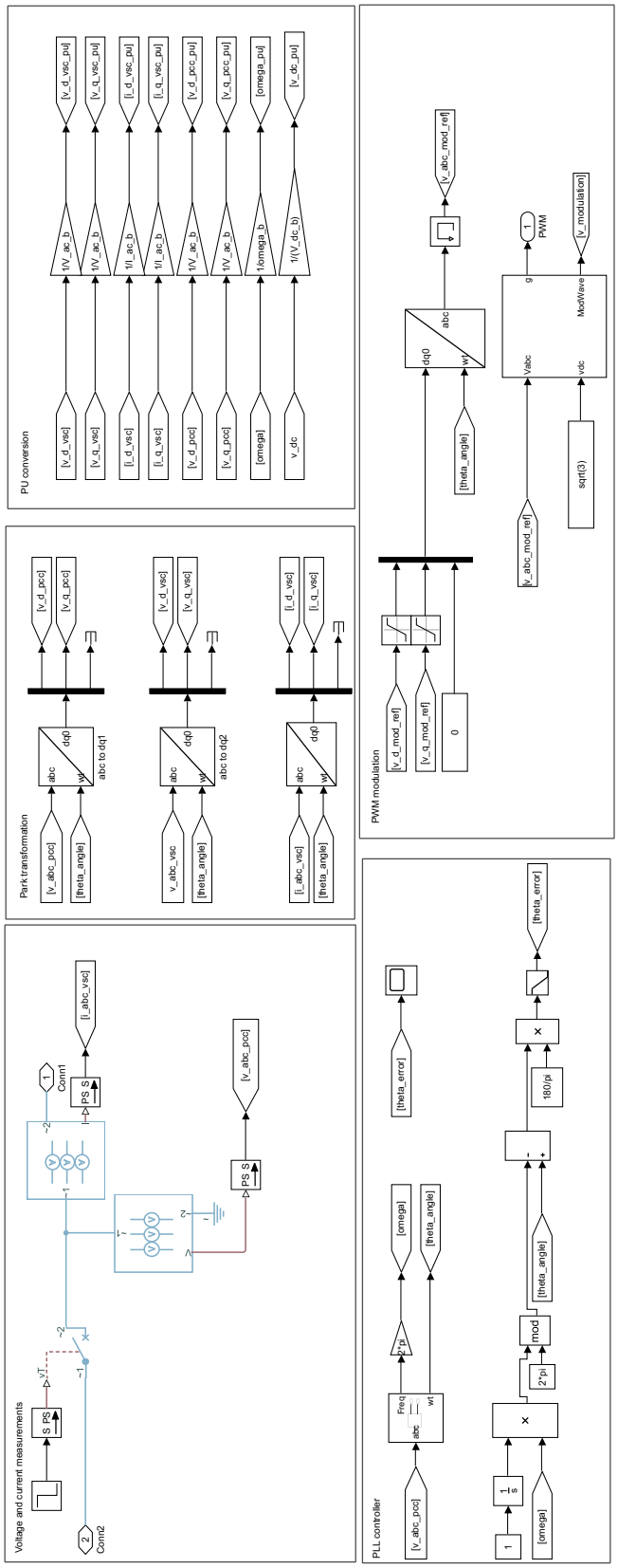

STATCOM-Inner & outer controller

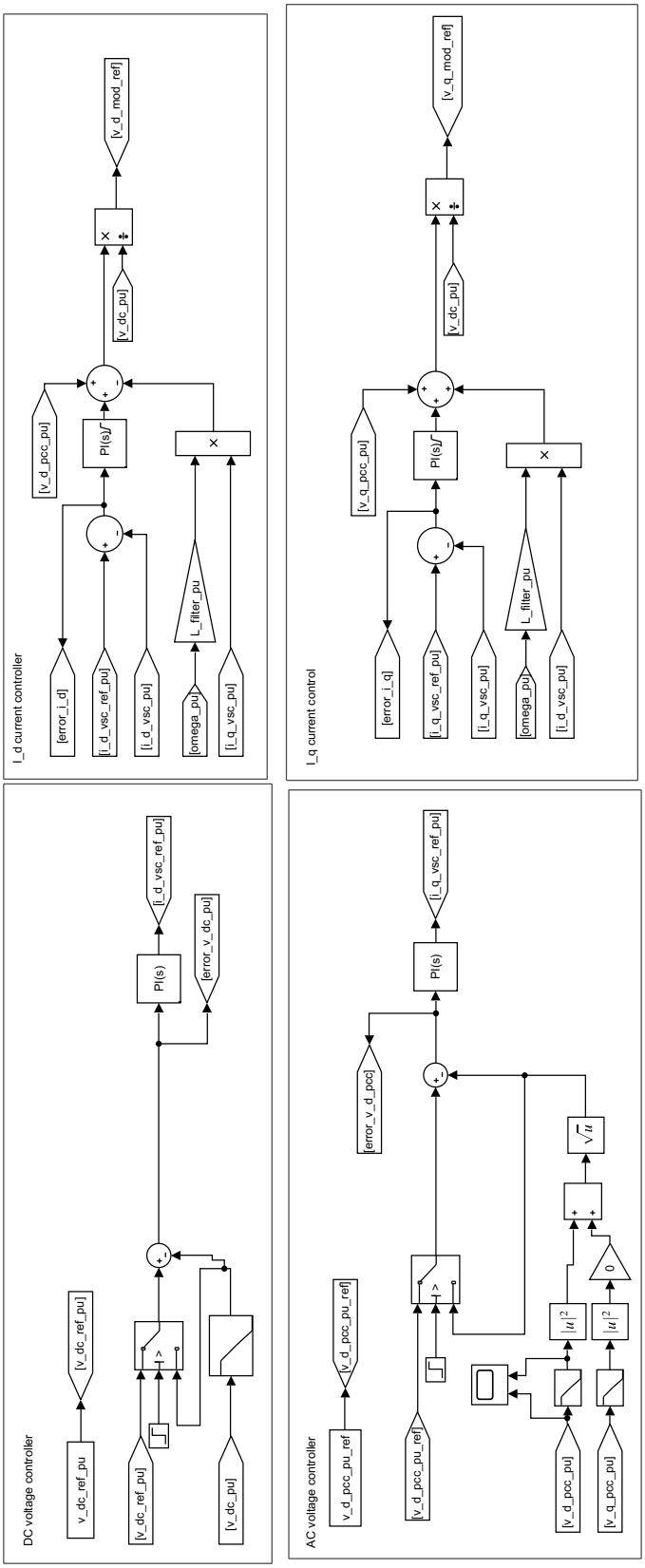

D.1 MATLAB scripts

MATPOWER

```
%% Title: Script initialization case grid Trondenergy:
%% Datum: 13/06/2018
%% Author: Adrien Karoui

%% 1 Data:

f=50 %Hz

%Per unit: Base value
S_base  =100*10^3 % VA
U_1_base= 22*10^3 %V
V_1_base=U_1_base*sqrt(3) %V
I_1_base=S_base/(sqrt(3)*U_1_base)% A
Z_1_base=U_1_base^2/S_base
Y_1_base=(1/Z_1_base)*1e9;

V_2_base=230 %V
U_2_base=sqrt(3)*V_2_base %V
I_2_base=S_base/(sqrt(3)*U_2_base)% A
Z_2_base=U_2_base^2/S_base
Y_2_base=(1/Z_2_base)*1e9;

%1.1) Cable Parameters
% Nomenclature:
% NAME_OF_CABLE=[Resistance[Ohm/km] reactance[Ohm/km]
    Line_Line_capacitance[nS/km] Line_ground_capacitance[nS/km]]

EX_1X25_data=[1.2 0.082 0.28*2*pi*f 0.552*2*pi*f];
EX_1X50_data=[0.641 0.077 0.412*2*pi*f 0.82*2*pi*f];
EX_1X95_data=[0.32 0.076 0.522*2*pi*f 1.092*2*pi*f];

AL_1X25_data=[0.717 0.345 4.32*2*pi*f 10.722*2*pi*f];
AL_1X50_data=[0.256 0.312 4.482*2*pi*f 11.912*2*pi*f];

TFXP_1X4X95_AL_data=[0.32 0.075 0.572*2*pi*f 1.12*2*pi*f];
TFXP_JETNET_1X4X50_data=[0.641 0.079 0.53*2*pi*f 1.08*2*pi*f];
TFLP_1X3X95_AL_data=[0.32 0.075 0.57*2*pi*f 1.1*2*pi*f]; % I could
    not find the right data out of the datasheet/internet

```

```
PFSP_1X3X25_AL_data=[1.2  0.082  0.42*2*pi*f  0.82*2*pi*f];
PFSP_1X3X50_AL_data=[0.641  0.079  0.53*2*pi*f  1.08*2*pi*f];

%1.2) Line paramater: [ line_length[km] Resistance[Ohm/km]
    reactance[Ohm/km] Line_Line_capacitance[nF/km]
    Line_ground_capacitance[nF/km] ]
%Zone A:
line_B1t_BA1 = horzcat(85*10^-3,TFXP_1X4X95_AL_data);
line_BA1_BA2=horzcat(252*10^-3,EX_1X95_data);
line_BA2_BA3a=horzcat(21*10^-3,EX_1X25_data);
line_BA2_BA3b=horzcat(12*10^-3,EX_1X25_data);
line_BA2_BA3c=horzcat(52*10^-3,EX_1X95_data);
line_BA3c_BA4a=horzcat(22*10^-3,PFSP_1X3X25_AL_data);
line_BA3c_BA4b=horzcat(60*10^-3,EX_1X95_data);
line_BA4b_BA5=horzcat(120*10^-3,EX_1X95_data);
line_BA5_BA6=horzcat(134*10^-3,EX_1X50_data);

%Zone B (indexed with C in data of the company):
line_B1t_BB1=horzcat(85*10^-3,TFXP_1X4X95_AL_data);
line_BB1_BB2=horzcat(664*10^-3,EX_1X95_data);
line_BB2_BB3a=horzcat(70*10^-3,EX_1X50_data);
line_BB2_BB3b=horzcat(194*10^-3,EX_1X50_data);
line_BB3a_BB4=horzcat(3*10^-3,TFLP_1X3X95_AL_data);
line_BB4_BB5a=horzcat(21*10^-3,PFSP_1X3X25_AL_data);
line_BB4_BB5b=horzcat(68*10^-3,PFSP_1X3X50_AL_data);

%Zone C (indexed with B in data of the company)::
line_B1t_BC1=horzcat(85*10^-3,TFXP_1X4X95_AL_data);
line_BC1_BC2=horzcat(54*10^-3,EX_1X95_data);
line_BC2_BC3=horzcat(130*10^-3,AL_1X50_data);
line_BC3_BC4=horzcat(178*10^-3,AL_1X25_data);
line_BC4_BC5a=horzcat(27*10^-3,EX_1X25_data);
line_BC4_BC5b=horzcat(77*10^-3,AL_1X25_data);
line_BC5a_BC6a=horzcat(21*10^-3,PFSP_1X3X25_AL_data);
line_BC5b_BC6b=horzcat(37*10^-3,EX_1X25_data);

%Modified line parameters:
line_B1t_BA1=horzcat(line_B1t_BA1, [line_B1t_BA1(1)*line_B1t_BA1
    (2) line_B1t_BA1(1)*line_B1t_BA1(3)]/Z_2_base, [line_B1t_BA1(1)*
    line_B1t_BA1(4) line_B1t_BA1(1)*line_B1t_BA1(5)]/Y_2_base);
line_BA1_BA2=horzcat(line_BA1_BA2, [line_BA1_BA2(1)*line_BA1_BA2
    (2) line_BA1_BA2(1)*line_BA1_BA2(3)]/Z_2_base, [line_BA1_BA2(1)*
    line_BA1_BA2(4) line_BA1_BA2(1)*line_BA1_BA2(5)]/Y_2_base);
```

```
75 line_BA2_BA3a=horzcat(line_BA2_BA3a, [line_BA2_BA3a(1)*
       line_BA2_BA3a(2) line_BA2_BA3a(1)*line_BA2_BA3a(3)]/Z_2_base, [
       line_BA2_BA3a(1)*line_BA2_BA3a(4) line_BA2_BA3a(1)*line_BA2_BA3a
       (5)]/Y_2_base);
76 line_BA2_BA3b=horzcat(line_BA2_BA3b, [line_BA2_BA3b(1)*
       line_BA2_BA3b(2) line_BA2_BA3b(1)*line_BA2_BA3b(3)]/Z_2_base, [
       line_BA2_BA3b(1)*line_BA2_BA3b(4) line_BA2_BA3b(1)*line_BA2_BA3b
       (5)]/Y_2_base);
77 line_BA2_BA3c=horzcat(line_BA2_BA3c, [line_BA2_BA3c(1)*
       line_BA2_BA3c(2) line_BA2_BA3c(1)*line_BA2_BA3c(3)]/Z_2_base, [
       line_BA2_BA3c(1)*line_BA2_BA3c(4) line_BA2_BA3c(1)*line_BA2_BA3c
       (5)]/Y_2_base);
78 line_BA3c_BA4a=horzcat(line_BA3c_BA4a, [line_BA3c_BA4a(1)*
       line_BA3c_BA4a(2) line_BA3c_BA4a(1)*line_BA3c_BA4a(3)]/Z_2_base,
        [line_BA3c_BA4a(1)*line_BA3c_BA4a(4) line_BA3c_BA4a(1)*
       line_BA3c_BA4a(5)]/Y_2_base);
79 line_BA3c_BA4b=horzcat(line_BA3c_BA4b, [line_BA3c_BA4b(1)*
       line_BA3c_BA4b(2) line_BA3c_BA4b(1)*line_BA3c_BA4b(3)]/Z_2_base,
        [line_BA3c_BA4b(1)*line_BA3c_BA4b(4) line_BA3c_BA4b(1)*
       line_BA3c_BA4b(5)]/Y_2_base);
80 line_BA4b_BA5=horzcat(line_BA4b_BA5, [line_BA4b_BA5(1)*
       line_BA4b_BA5(2) line_BA4b_BA5(1)*line_BA4b_BA5(3)]/Z_2_base, [
       line_BA4b_BA5(1)*line_BA4b_BA5(4) line_BA4b_BA5(1)*line_BA4b_BA5
       (5)]/Y_2_base);
81 line_BA5_BA6=horzcat(line_BA5_BA6, [line_BA5_BA6(1)*line_BA5_BA6
       (2) line_BA5_BA6(1)*line_BA5_BA6(3)]/Z_2_base, [line_BA5_BA6(1)*
       line_BA5_BA6(4) line_BA5_BA6(1)*line_BA5_BA6(5)]/Y_2_base);
82
83 line_B1t_BB1=horzcat(line_B1t_BB1, [line_B1t_BB1(1)*line_B1t_BB1
       (2) line_B1t_BB1(1)*line_B1t_BB1(3)]/Z_2_base, [line_B1t_BB1(1)*
       line_B1t_BB1(4) line_B1t_BB1(1)*line_B1t_BB1(5)]/Y_2_base);
84 line_BB1_BB2=horzcat(line_BB1_BB2, [line_BB1_BB2(1)*line_BB1_BB2
       (2) line_BB1_BB2(1)*line_BB1_BB2(3)]/Z_2_base, [line_BB1_BB2(1)*
       line_BB1_BB2(4) line_BB1_BB2(1)*line_BB1_BB2(5)]/Y_2_base);
85 line_BB2_BB3a=horzcat(line_BB2_BB3a, [line_BB2_BB3a(1)*
       line_BB2_BB3a(2) line_BB2_BB3a(1)*line_BB2_BB3a(3)]/Z_2_base, [
       line_BB2_BB3a(1)*line_BB2_BB3a(4) line_BB2_BB3a(1)*line_BB2_BB3a
       (5)]/Y_2_base);
86 line_BB2_BB3b=horzcat(line_BB2_BB3b, [line_BB2_BB3b(1)*
       line_BB2_BB3b(2) line_BB2_BB3b(1)*line_BB2_BB3b(3)]/Z_2_base, [
       line_BB2_BB3b(1)*line_BB2_BB3b(4) line_BB2_BB3b(1)*line_BB2_BB3b
       (5)]/Y_2_base);
```

```
87 line_BB3a_BB4=horzcat(line_BB3a_BB4, [line_BB3a_BB4(1)*
       line_BB3a_BB4(2) line_BB3a_BB4(1)*line_BB3a_BB4(3)]/Z_2_base, [
       line_BB3a_BB4(1)*line_BB3a_BB4(4) line_BB3a_BB4(1)*line_BB3a_BB4
       (5)]/Y_2_base);
88 line_BB4_BB5a=horzcat(line_BB4_BB5a, [line_BB4_BB5a(1)*
       line_BB4_BB5a(2) line_BB4_BB5a(1)*line_BB4_BB5a(3)]/Z_2_base, [
       line_BB4_BB5a(1)*line_BB4_BB5a(4) line_BB4_BB5a(1)*line_BB4_BB5a
       (5)]/Y_2_base);
89 line_BB4_BB5b=horzcat(line_BB4_BB5b, [line_BB4_BB5b(1)*
       line_BB4_BB5b(2) line_BB4_BB5b(1)*line_BB4_BB5b(3)]/Z_2_base, [
       line_BB4_BB5b(1)*line_BB4_BB5b(4) line_BB4_BB5b(1)*line_BB4_BB5b
       (5)]/Y_2_base);
90
91 line_B1t_BC1=horzcat(line_B1t_BC1, [line_B1t_BC1(1)*line_B1t_BC1
       (2) line_B1t_BC1(1)*line_B1t_BC1(3)]/Z_2_base, [line_B1t_BC1(1)*
       line_B1t_BC1(4) line_B1t_BC1(1)*line_B1t_BC1(5)]/Y_2_base);
92 line_BC1_BC2=horzcat(line_BC1_BC2, [line_BC1_BC2(1)*line_BC1_BC2
       (2) line_BC1_BC2(1)*line_BC1_BC2(3)]/Z_2_base, [line_BC1_BC2(1)*
       line_BC1_BC2(4) line_BC1_BC2(1)*line_BC1_BC2(5)]/Y_2_base);
93 line_BC2_BC3=horzcat(line_BC2_BC3, [line_BC2_BC3(1)*line_BC2_BC3
       (2) line_BC2_BC3(1)*line_BC2_BC3(3)]/Z_2_base, [line_BC2_BC3(1)*
       line_BC2_BC3(4) line_BC2_BC3(1)*line_BC2_BC3(5)]/Y_2_base);
94 line_BC3_BC4=horzcat(line_BC3_BC4, [line_BC3_BC4(1)*line_BC3_BC4
       (2) line_BC3_BC4(1)*line_BC3_BC4(3)]/Z_2_base, [line_BC3_BC4(1)*
       line_BC3_BC4(4) line_BC3_BC4(1)*line_BC3_BC4(5)]/Y_2_base);
95 line_BC4_BC5a=horzcat(line_BC4_BC5a, [line_BC4_BC5a(1)*
       line_BC4_BC5a(2) line_BC4_BC5a(1)*line_BC4_BC5a(3)]/Z_2_base, [
       line_BC4_BC5a(1)*line_BC4_BC5a(4) line_BC4_BC5a(1)*line_BC4_BC5a
       (5)]/Y_2_base);
96 line_BC4_BC5b=horzcat(line_BC4_BC5b, [line_BC4_BC5b(1)*
       line_BC4_BC5b(2) line_BC4_BC5b(1)*line_BC4_BC5b(3)]/Z_2_base, [
       line_BC4_BC5b(1)*line_BC4_BC5b(4) line_BC4_BC5b(1)*line_BC4_BC5b
       (5)]/Y_2_base);
97 line_BC5a_BC6a=horzcat(line_BC5a_BC6a, [line_BC5a_BC6a(1)*
       line_BC5a_BC6a(2) line_BC5a_BC6a(1)*line_BC5a_BC6a(3)]/Z_2_base,
        [line_BC5a_BC6a(1)*line_BC5a_BC6a(4) line_BC5a_BC6a(1)*
       line_BC5a_BC6a(5)]/Y_2_base);
98 line_BC5b_BC6b=horzcat(line_BC5b_BC6b, [line_BC5b_BC6b(1)*
       line_BC5b_BC6b(2) line_BC5b_BC6b(1)*line_BC5b_BC6b(3)]/Z_2_base,
        [line_BC5b_BC6b(1)*line_BC5b_BC6b(4) line_BC5b_BC6b(1)*
       line_BC5b_BC6b(5)]/Y_2_base);
99
100
```

```
101
102
103
104
105
106
107
108
109 %1.3) Load:
110 %Nomenclature: S_name_load=[V_rated[line to line kV] P_load[W]
        Q_load[var]]
111
112 %zone A:
113 S_LA3a=[0.23 3.7*10^3 0.75*10^3];
114 S_LA3b=[0.23 3.7*10^3 0.75*10^3];
115 S_LA4a=[0.23 0.394*10^3 0.08*10^3];
116 S_LA6=[0.23 6.516*10^3 1.323*10^3];
117
118 %zone B:
119 S_LB3b=[0.23 0.1 0.1];
120 S_LB5a=[0.23 6.141*10^3 1.247*10^3];
121 S_LB5b=[0.23 0.1 0.1];
122
123
124 %zone C:
125 S_LC6a=[0.23 2.186*10^3 0.444*10^3];
126 S_LC6b=[0.23 0.095*10^3 0.019*10^3];
127
128
129
130 %1.4) Stiff network (E_network & X_network):
131
132 S_cc=1000*10^3 %VA
133 S_cc_pu=S_cc/S_base % pu
134
135 X_net_pu=1/S_cc_pu% pu
136 X_net=X_net_pu*Z_1_base %Ohm
137 L_net=X_net/(2*pi*f)%H
```

```
%% Title: Trondenergy_case MATPOWER function
%% Datum: 13/06/2018
%% Author: Adrien Karoui



function mpc = trondenergy_case
%CASE Trondenergy    Power flow data 26 buses
%   Please see CASEFORMAT for details on the case file format.
%
%   Based on data from Joe H. Chow's book, p. 70.

%   MATPOWER

run('script_case_study_trondEnergy_for_matpower');

%% MATPOWER Case Format : Version 2
mpc.version = '2';

%%-----  Power Flow Data  -----%%
%% system MVA base
mpc.baseMVA = 100e-3;

%% bus data
% bus_i type Pd Qd  Gs  Bs  area  Vm  Va  baseKV  zone  Vmax  Vmin
mpc.bus = [
        1 3 0 0 0 0 1 1 0 22      2 1.1 0.9;
        2 2 0 0 0 0 1 1 0 0.23  1 1.1 0.9;
        3 2 0 0 0 0 1 1 0 0.23  1 1.1 0.9;
        4 2 0 0 0 0 1 1 0 0.23  1 1.1 0.9;
        5 1 S_LA3a(2)*1e-6  S_LA3a(3)*1e-6  0 0 1 1 0 0.23  1 1.1
            0.9;
        6 1 S_LA3b(2)*1e-6  S_LA3b(3)*1e-6  0 0 1 1 0 0.23  1 1.1
            0.9;
        7 2 0 0 0 0 1 1 0 0.23  1 1.1 0.9;
        8 1 S_LA4a(2)*1e-6  S_LA4a(3)*1e-6  0 0 1 1 0 0.23  1 1.1
            0.9;
        9 2 0 0 0 0 1 1 0 0.23  1 1.1 0.9;
        10  2 0 0 0 0 1 1 0 0.23  1 1.1 0.9;
        11  1 S_LA6(2)*1e-6 S_LA6(3)*1e-6 0 0 1 1 0 0.23  1 1.1
            0.9;
        12  2 0 0 0 0 1 1 0 0.23  1 1.1 0.9;
        13  2 0 0 0 0 1 1 0 0.23  1 1.1 0.9;
```

```
40          14  1 S_LB3b(2)*1e-6  S_LB3b(3)*1e-6  0 0 1 1 0 0.23  1
               1.1  0.9;
41          15  2 0 0 0 0 1 1 0 0.23  1 1.1  0.9;
42          16  2 0 0 0 0 1 1 0 0.23  1 1.1  0.9;
43          17  1 S_LB5a(2)*1e-6  S_LB5a(3)*1e-6  0 0 1 1 0 0.23  1
               1.1  0.9;
44          18  1 S_LB5b(2)*1e-6  S_LB5b(3)*1e-6  0 0 1 1 0 0.23  1
               1.1  0.9;
45          19  2 0 0 0 0 1 1 0 0.23  1 1.1  0.9;
46          20  2 0 0 0 0 1 1 0 0.23  1 1.1  0.9;
47          21  2 0 0 0 0 1 1 0 0.23  1 1.1  0.9;
48          22  2 0 0 0 0 1 1 0 0.23  1 1.1  0.9;
49          23  2 0 0 0 0 1 1 0 0.23  1 1.1  0.9;
50          24  2 0 0 0 0 1 1 0 0.23  1 1.1  0.9;
51          25  1 S_LC6a(2)*1e-6  S_LC6a(3)*1e-6    0 0 1 1 0 0.23  1
               1.1  0.9;
52          26  1 S_LC6b(2)*1e-6  S_LC6b(3)*1e-6  0 0 1 1 0 0.23  1
               1.1  0.9;
53  ];
54
55  %% generator data
56  % bus Pg  Qg  Qmax  Qmin  Vg  mBase status  Pmax  Pmin  Pc1 Pc2
       Qc1min  Qc1max  Qc2min  Qc2max  ramp_agc  ramp_10 ramp_30 ramp_q
         apf
57  mpc.gen = [
58    1 0 0 30  -30 1 1 1 40  0 0 0 0 0 0 0 0 0 0 0 0;
59  %   2 163 0 300 -300  1 100 1 300 10  0 0 0 0 0 0 0 0 0 0 0;
60  %   3 85  0 300 -300  1 100 1 270 10  0 0 0 0 0 0 0 0 0 0 0;
61  ];
62
63  %% branch data
64  % fbus  tbus  r x b rateA rateB rateC ratio angle status  angmin
       angmax
65  mpc.branch = [
66    1 2 0.01  0.1 0 0 0 0 1 0 1 -360  360;
67    2 3 line_B1t_BA1(6) line_B1t_BA1(7) line_B1t_BA1(9) 0 0 0 0 0 1
         -360  360;
68    3 4 line_BA1_BA2(6) line_BA1_BA2(7) line_BA1_BA2(9) 0 0 0 0 0 1
         -360  360;
69    4 5 line_BA2_BA3a(6)  line_BA2_BA3a(7)  line_BA2_BA3a(9)  0 0 0
         0 0 1 -360  360;
70    4 6 line_BA2_BA3b(6)  line_BA2_BA3b(7)  line_BA2_BA3b(9)  0 0 0
         0 0 1 -360  360;
```

```
71   4  7 line_BA2_BA3c(6)   line_BA2_BA3c(7)   line_BA2_BA3c(9)   0 0 0
        0 0 1 -360  360;
72   7  8 line_BA3c_BA4a(6) line_BA3c_BA4a(7) line_BA3c_BA4a(9) 0 0 0
        0 0 1 -360  360;
73   7  9 line_BA3c_BA4b(6) line_BA3c_BA4b(7) line_BA3c_BA4b(9) 0 0 0
        0 0 1 -360  360;
74   9 10  line_BA4b_BA5(6)  line_BA4b_BA5(7)  line_BA4b_BA5(9)  0 0
        0 0 0 1 -360  360;
75     10  11  line_BA5_BA6(6) line_BA5_BA6(7) line_BA5_BA6(9) 0 0 0
          0 0 1 -360  360;
76   2 12  line_B1t_BB1(6) line_B1t_BB1(7) line_B1t_BB1(9) 0 0 0 0 0
        1 -360  360;
77   12  13  line_BB1_BB2(6) line_BB1_BB2(7) line_BB1_BB2(9) 0 0 0 0
        0 1 -360  360;
78   13  14  line_BB2_BB3b(6)  line_BB2_BB3b(7)  line_BB2_BB3b(9)  0
        0 0 0 0 1 -360  360;
79   13  15  line_BB2_BB3a(6)  line_BB2_BB3a(7)  line_BB2_BB3a(9)  0
        0 0 0 0 1 -360  360;
80   15  16  line_BB3a_BB4(6)  line_BB3a_BB4(7)  line_BB3a_BB4(9)  0
        0 0 0 0 1 -360  360;
81   16  17  line_BB4_BB5a(6)  line_BB4_BB5a(7)  line_BB4_BB5a(9)  0
        0 0 0 0 1 -360  360;
82   16  18  line_BB4_BB5b(6)  line_BB4_BB5b(7)  line_BB4_BB5b(9)  0
        0 0 0 0 1 -360  360;
83   2 19  line_B1t_BC1(6) line_B1t_BC1(7) line_B1t_BC1(9) 0 0 0 0 0
        1 -360  360;
84   19  20  line_BC1_BC2(6) line_BC1_BC2(7) line_BC1_BC2(9) 0 0 0 0
        0 1 -360  360;
85   20  21  line_BC2_BC3(6) line_BC2_BC3(7) line_BC2_BC3(9) 0 0 0 0
        0 1 -360  360;
86   21  22  line_BC3_BC4(6) line_BC3_BC4(7) line_BC3_BC4(9) 0 0 0 0
        0 1 -360  360;
87   22  23  line_BC4_BC5a(6)  line_BC4_BC5a(7)  line_BC4_BC5a(9)  0
        0 0 0 0 1 -360  360;
88   22  24  line_BC4_BC5b(6)  line_BC4_BC5b(7)  line_BC4_BC5b(9)  0
        0 0 0 0 1 -360  360;
89   23  25  line_BC5a_BC6a(6) line_BC5a_BC6a(7) line_BC5a_BC6a(9) 0
        0 0 0 0 1 -360  360;
90   24  26  line_BC5b_BC6b(6) line_BC5b_BC6b(7) line_BC5b_BC6b(9) 0
        0 0 0 0 1 -360  360;
91 ];
92
93 %%-----  OPF Data  -----%%
```

```
94 %% generator cost data
95 % 1 startup shutdown  n x1  y1  ... xn  yn
96 % 2 startup shutdown  n c(n-1)  ... c0
97 mpc.gencost = [
98   2 1500  0 3 0.11  5 150;
99 %   2 2000  0 3 0.085 1.2 600;
100 %   2 3000  0 3 0.1225  1 335;
101 ];
```

Magnetic Voltage Booster

```
%% Title: MVB simscape script model
%% Datum: 13/06/2018
%% Author: Adrien Karoui


component MVB_Model_final

nodes
    p_in = foundation.electrical.electrical; % +in:left
    n_grd = foundation.electrical.electrical; % -in:left
    p_out = foundation.electrical.electrical; % +out:right
end

parameters
    n = 1;   % Winding ratio in [0,1]
end

variables
    i_in = {1 , 'A' }; % Input current
    v_in = { 1, 'V' }; % Input voltage
    i_out = {1, 'A' }; % Output current
    v_out = { 1, 'V' }; % Output voltage
    i_m =  { 1, 'A' }; % variable inductance current
    v_3 =  { 1, 'V' }; % variable inductance voltage
    v_1 = { 1, 'V' }; % Auto transformer output voltage
    v_2 = { 1, 'V' }; % Auto transformer input voltage
end

outputs
    i_in_res = { 1, 'A' };   % Input current
    i_out_res = { 1, 'A' };  % Output current
    i_m_res =  { 1, 'A' };   % variable inductance current
    v_in_res = { 1, 'V' };   % Input voltage
    v_out_res = { 1, 'V' };  % Output voltage
    v_1_res = { 1, 'V' };    % Auto transformer primary voltage
    v_2_res = { 1, 'V' };    % Auto transformer secondary voltage
    v_3_res =  { 1, 'V' };   % variable inductance voltage
end

inputs
   L_m= { 10, 'H' }; % Variable Inductance
```

```
42 end
43 branches
44     i_out : p_in.i -> p_out.i;
45     i_m : p_in.i -> n_grd.i;
46 end
47
48 equations
49     v_in == p_in.v - n_grd.v;
50     v_out == p_out.v - n_grd.v;
51     v_in ==v_2+v_3;
52     v_3 ==L_m*i_m.der;
53     i_in==i_out+i_m;
54     v_out==v_1+v_in;
55     v_2==n*v_1;
56     i_out==i_m/n;
57
58     i_in_res == i_in;
59     v_in_res == v_in;
60     i_out_res == i_out;
61     v_out_res == v_out;
62     i_m_res ==  i_m;
63     v_2_res == v_2;
64     v_1_res == v_1;
65     v_3_res== v_3
66 end
67
68 end
```

STATCOM

```
%% Title: STATCOM initialization script
%% Date : 13/06/2018
%% Author: Adrien Karoui



%% Per unit: Base value
S_b=100*10^3          % VA
f_b= 50               %Hz
omega_b=2*pi*f_b      %rad/s
%High voltage side
V_1_base=22*10^3              %V RMS line to ground
I_1_base=S_b/(3*V_1_base)     % A
Z_1_base=V_1_base/I_1_base; % Ohm

%Low voltage side: network
V_2_base=230                  % V RMS line to ground
I_2_base=S_b/(3*V_2_base)  % A
Z_2_base=V_2_base/I_2_base % Ohm

%% Stiffness network (E_network & X_network):
S_cc_pu=5          % pu
S_cc=S_cc_pu*S_b %VA

%% Fault Timing
fault_start_time=0.6     %second
fault_clearing_time=0.7 %second

%% Statcom
connection_time_statcom=0.5                %second
connection_time_statcom_controller=0.5  %second

% Per unitize:
% AC side:
V_ac_b=sqrt(2)*V_2_base; %V (peak value)
I_ac_b=2*S_b/(3*V_ac_b); %A (peak value)
Z_ac_b=V_ac_b/I_ac_b;     %Ohm
R_ac_b=Z_ac_b;            %Ohm
L_ac_b=Z_ac_b/omega_b;    %H
C_ac_b=1/(omega_b*Z_ac_b)%F

```

```
% DC side:
V_dc_b=2*V_ac_b;        %V
I_dc_b=S_b/V_dc_b;      %A
Z_dc_b=V_dc_b/I_dc_b;   %Ohm
L_dc_b=(8/3)*L_ac_b;    %H
C_dc_b=(3/8)*C_ac_b     %F

%% Statcom characteristic
L_filter_pu=0.3;     % pu ok pour le parametre
R_filter_pu=0.1      %pu
C_dc_pu=10           %pu

L_filter=L_filter_pu*L_ac_b; %H
R_filter=R_filter_pu*R_ac_b  %Ohm
C_dc=C_dc_pu*C_dc_b          %F
v_C_dc_ini=V_dc_b            %V

%per unit
v_dc_ref_pu=v_C_dc_ini/V_dc_b % pu
v_d_pcc_pu_ref=1               % pu


%% Design of the inner current controller (Santiago Method):

T_f=0.0001 %s switching time consntant

%D-axis current controller
k_p_d=L_filter_pu/(2*omega_b*T_f);
k_i_d=R_filter_pu/(2*T_f);

%Q-axis current controller
k_p_q=k_p_d;
k_i_q=k_i_d;
```

Bibliography

[1] R. D. Zimmerman, C. E. Murillo-Sanchez, and R. J. Thomas. "MATPOWER: Steady-State Operations, Planning, and Analysis Tools for Power Systems Research and Education". In: *IEEE Transactions on Power Systems* 26.1 (Feb. 2011), pp. 12–19. ISSN: 0885-8950. DOI: 10.1109/TPWRS.2010.2051168.

[2] The MathWorks R2018a. *How Simscape Simulation Works*. MathWorks, 1995. URL: https://nl.mathworks.com/help/physmod/simscape/ug/how-simscape-models-represent-physical-systems.html.

[3] L. Shampine, M. Reichelt, and J. Kierzenka. "Solving Index-1 DAEs in MATLAB and Simulink". In: *SIAM Review* 41.3 (1999), pp. 538–552. DOI: 10.1137/S003614459933425X. eprint: https://doi.org/10.1137/S003614459933425X. URL: https://doi.org/10.1137/S003614459933425X.

[4] Van Cutsem Thierry. *ELEC0047- Power system dynamics, control and stability, Behaviour of the synchronous machine during short circuit, Numerical Solution of the DAEs*. Oct. 2017.

[5] Van Cutsem Thierry. *ELEC0014 - Introduction to electric power and energy systems Some properties of electric energy transmission*. Sept. 2016.

[6] The MathWorks R2018a. *Transmission Line*. MathWorks, 1995. URL: https://nl.mathworks.com/help/physmod/sps/ref/transmissionline.html?s_tid=doc_ta.

[7] M. C. Tavares, J. Pissolato, and C. M. Portela. "New mode domain multiphase transmission line model-Clarke transformation evaluation". In: *Power System Technology, 1998. Proceedings. POWERCON '98. 1998 International Conference on*. Vol. 2. Aug. 1998, 860–864 vol.2. DOI: 10.1109/ICPST.1998.729207.

[8] *Power System Stability And Control*. EPRI power system engineering series. McGraw-Hill, 1994. ISBN: 9780070635159. URL: https://books.google.no/books?id=v3RxH%5C_GkwmsC.

[9] J. Machowski et al. *Power System Dynamics and Stability*. Wiley, 1997. ISBN: 9780471956433. URL: https://books.google.no/books?id=L7o4TitajRIC.

[10] Patricio Salmerón Revuelta, Salvador Pérez Litrán, and Jaime Prieto Thomas. "3 - Instantaneous Reactive Power Theory". In: *Active Power Line Conditioners*. Ed. by Patricio Salmerón Revuelta, Salvador Pérez Litrán, and Jaime Prieto Thomas. San Diego: Academic Press, 2016, pp. 51–105. ISBN: 978-0-12-803216-9. DOI: https://doi.org/10.1016/B978-0-12-803216-9.00003-1. URL: https://www.sciencedirect.com/science/article/pii/B9780128032169000031.

[11] Van Cutsem Thierry. *Dynamic of the induction machine*. Oct. 2017.

[12] Espen Haugs and Frank Strand. *Magnetically influenced current or voltage regulatro and magnetically influenced converter*. Aug. 2005.

[13] J. Avila-Montes et al. "A Novel Compensation Scheme Based on a Virtual Air Gap Variable Reactor for AC Voltage Control". In: *IEEE Transactions on Industrial Electronics* 61.12 (Dec. 2014), pp. 6547–6555. ISSN: 0278-0046. DOI: 10.1109/TIE.2014.2321335.

[14] *Magtech Voltage Booster Stabilising medium voltage lines*. TJA1043. Rev. 3. MagtechAS. Apr. 2013. URL: https://www.slo.lv/upload/catalog/vidspriegums/magtech_voltage_booster_medium_290311_eng.pdf.

[15] The MathWorks R2018a. *PWM Generator (Three-phase, Two-level)*. MathWorks, 1995. URL: https://nl.mathworks.com/help/physmod/sps/ref/pwmgeneratorthreephas%5C%5Cetwolevel.html?searchHighlight=SPWM&s_tid=doc_srchtitle.

[16] Andrezj M. Trzynadlowski. *Introduction to modern power electronics, 2nd edition*. Wiley, 2010. ISBN: 97804704001033.

[17] Amirnaser Yazdani. *Voltage-sourced converters in power systems : modeling, control, and applications*. eng. Hoboken, N.J., 2010.

[18] The MathWorks R2018a. *PLL (3phi)*. MathWorks, 1995. URL: https://se.mathworks.com/help/physmod/sps/powersys/ref/pll3ph.html?searchHighlight=PLL&s_tid=doc_srchtitle.

[19] D. Zhang and J. Fletcher. "Modeling a DC-current-controlled variable inductance and its application to grid-tied converters". In: *2016 IEEE International Conference on Power System Technology (POWERCON)*. Sept. 2016, pp. 1–5. DOI: 10.1109/POWERCON.2016.7754075.

[20] *RENBLAD Distribusjonsnett – Tekniske verdier*. 8041. VER. 3.1. Rasjonell Elektrisk Nettvirksomhet. 2011.

[21] *Kabelboka Håndbok for e-verkskabler*. 8041. VER. 3.1. NEXANS NORWAY AS. 2011. URL: https://www.nexans.no/eservice/Norway-no_NO/fileLibrary/Download_540200470/Norway/files/Nexans_Kabelboka_e-verk_2014.pdf.

[22] *Magtech^{TM}. Magtech Voltage Booster Spenningsstabilisering i lavspentnett*. July 2016.

[23] S. Sanchez, G. Bergna, and E. Tedeschi. "Tuning of control loops for grid-connected Modular Multilevel Converters under a simplified port representation for large system studies". In: *2017 Twelfth International Conference on Ecological Vehicles and Renewable Energies (EVER)*. Apr. 2017, pp. 1–8. DOI: 10.1109/EVER.2017.7935913.